École polytechnique de Louvain

Design of a Robot for Assisting Handwriting in Children with Dyslexia

Author: **Antonin Perilleux**
Supervisor: **Renaud Ronsse**
Readers: **Renaud Ronsse, Benoît Herman, Julien Guiaux Brinon**
Academic year 2024–2025
Master [120] in Electro-mechanical Engineering

Contents

1 Introduction

This master's thesis presents the design of a handwriting assistance robot for children with dysgraphia. This topic falls within the field of Human-Robot Interaction (HRI). A state-of-the-art section will explore the concept of HRI and existing robots that are similar in purpose.

To begin any design process, it is important to understand the need. A detailed explanation of the context in which this idea emerged is first provided. The goal of the robot is to help children develop motor patterns to improve their handwriting. The problem and associated needs are translated into a specification sheet. To quantify certain values within it, data analysis was performed. This specification sheet defines the robot's performance requirements and serves as a basis for design.

Once the specifications are set, the design phase begins. First, the general concept must be selected from different alternatives, based on defined criteria. While detailed aspects are not yet addressed at this stage, a first sketch of the robot can already be established.

After the concept is chosen, the design is refined. This includes the selection of components such as motors, supports, sensors, and others. The robot is then modeled in SolidWorks to create a virtual twin of the system. A list of required components and suppliers is created, along with the list of parts that need to be manufactured. This concludes the work presented in this Master's thesis.

2 State of the Art

Robots have been around for a few decades now, mainly in the industrial world, performing automated tasks to compensate for the lack or high cost of personnel and to fulfil the desire to automatize daily and repeatable tasks. Nowadays they are progressively coming into our daily lives to assist in some of our routine tasks—vacuum cleaner robots or mowing robots are good examples of this. The next major development in robotics is their interaction with humans, giving rise to the field of physical Human-Robot Interaction (pHRI). Applications are diverse and not limited to any particular domain; robots can be integrated into nearly every aspect of life, from logistics and healthcare to domestic and assistive services, as illustrated in Figure 1.

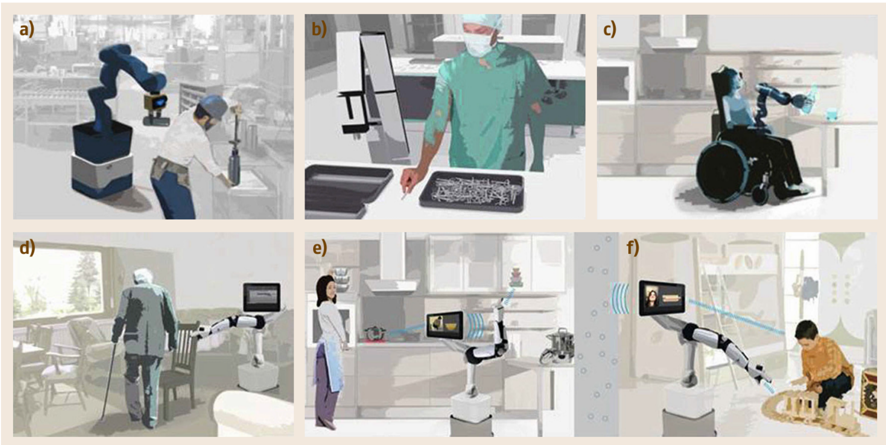

Figure 1: Application examples from [1]: manipulation and logistics (a, b), assistance for disabled or elderly individuals (c, d), and domestic service robots(e,f)

2.1 Classification

According to Haddadin et al.[1], Physical Human-Robot Interaction can be classified into three sub-categories: *cooperative*, *supportive*, and *collaborative*, based on the type of interaction the robot has with the human user..

1. *Supportive:* Supportive human-robot interactions are ones where the robot plays an active part in the task. As the name suggests, the robot supports the human in accomplishing a task. Examples of such robots include museum tour robots, or mobile manipulators for the disabled and elderly that can move around the house, monitor individuals, and fetch objects. These robots mostly avoid collisions with the environment and the human.

2. *Collaborative:* Collaborative human-robot interactions are those where humans and robots work together to achieve a shared task, with the work divided between them, each being best suited for their respective sub-tasks. They share the workspace and their interactions are planned. In these kinds of interactions, the human typically handles decision-making or dexterous tasks, while the robot performs repetitive, high-force, or precision-based operations.

3. *Cooperative:* Cooperative interactions involve the human and the robot working together simultaneously on the same task. Unlike collaborative robots (co-bots), cooperative robots manipulate the same object at the same time and actively participate in the task. Contact between the robot and human is continuous, through either a shared object or direct contact. Applications include kinesthetic teaching, coordinated material handling, and rehabilitation therapy.

The robot developed in this work falls into the cooperative interaction category. The user and the robot work together in completing the same task within a shared workspace. Their actions are simultaneous and physically coupled through a common object: the pen.

2.2 Safety

Safety can be addressed at different levels and at various stages throughout the design and use of a robot. The first level of consideration concerns the mechanical design, followed by motion planning, and finally the robot's control strategy [2].

De Luca et al. [3], in Integrated Control for pHRI: Collision Avoidance, Detection, Reaction and Collaboration, propose a model based on nested layers of behavior that the robot must achieve. The outermost layer corresponds to collaboration, involving interaction with the human and the execution of shared tasks. Nested within this is the layer of coexistence, where the robot and the human share the environment. At the core lies the safety layer, which encompasses all mechanisms and strategies ensuring safe operation during human-robot interaction.

In the context of this work, only the mechanical aspect of this safety framework is of direct relevance. Control strategies, motion planning, and reflex-like behaviors are outside the scope of the system, which focuses on ensuring passive safety through design choices.

Mechanical Design

When designing a robot for physical Human-Robot Interaction, safety plays a critical role in shaping design choices. For instance, sharp edges must be avoided to prevent skin puncture or laceration in the event of a collision. Moving parts should be kept as lightweight and low-inertia[2][1] as possible to minimize the risk of injury upon contact. Compliant mechanisms, such as soft materials and flexible transmissions[2], should also be integrated to absorb shocks and increase passive safety.

Additionally, motors can be relocated to the base—the stationary part of the robot—to reduce the mass and inertia of moving links. Transmission to the joints can then be achieved using cables and pulleys or belt systems[1]. These safety-oriented design elements fall under the category of passive safety and must be complemented by active safety strategies, which are implemented through sensor systems and control algorithms. Flexible design are also an other solution they can be implemented[1]:

- **Actively**, where compliance is generated by the control algorithm;
- **Passively**, where compliance arises from the mechanical structure (e.g., flexible joints or links).

Sensors and Active Safety

The design process also involves the strategic placement of sensors. A distinction can be made between embedded (onboard) sensors and external sensors, although their objective is the same: to collect information about the environment, enabling the robot controller to adapt behaviour in real time and ensure safe human-robot interaction—particularly by avoiding collisions.

Various types of sensors can be used, including range sensors, proximity sensors, tactile sensors, vision systems, audio sensors, and temperature sensors[2]. The robot should be equipped with a sensor configuration that maximizes environmental awareness, allowing it to accurately map its surroundings and react appropriately to changes.

The reactivity of sensors is also a critical parameter: high-speed response is essential to detect unexpected events and prevent collisions or accidents in dynamic environments. Furthermore, detecting and handling such unexpected events is a core requirement for ensuring operational safety.

Vision-based sensors[1][4][2], for example, can help define a dynamic "safety volume" around the robot, within which the system adjusts its behavior—such as reducing speed—when a human approaches. Among all sensor types, force and torque sensors[2] [1][4][5]are especially important in pHRI applications, as they are central to control strategies that involve continuous physical interaction. This topic will be further developed in the control section.

In general, using a diverse set of complementary sensors is strongly recommended when designing pHRI-capable robots. This increases robustness, improves situational awareness, and allows for compensation of individual sensor limitations through redundancy. Finally, the placement of sensors is equally important: they must be positioned where they can optimally detect relevant changes in the environment or interaction forces, such as at the end-effector, along the links, or within the workspace itself.

In the design of the handwriting assisting robot, the notions of active and passive safety are at its core. The robot's design must always consider the safety of its user. Light materials are used to ensure low inertia of the moving parts, sensors are included to provide knowledge of the surroundings and the user's movements, and compliance is integrated to increase safety. Cooperation with the user is continuous and occurs in close proximity, which makes safety even more important.

This work's application does not differ from most other pHRI systems, as force sensors are likely to be used for the control of the robot, as discussed further in this section. Motor encoders are also sensors that can be used to measure the position of the robot without being bulky or requiring direct visibility or large detection ranges.

2.3 Control

To control a robot in a physical Human-Robot Interaction context, the first strategies that come to mind are position control and force control.

In this section, the terms $\boldsymbol{x}$, $\boldsymbol{x}_d$, $\boldsymbol{x}_0$, and $\boldsymbol{q}_d$ are used in different equations. Here is a clarification of their meanings: $\boldsymbol{x}$ represents the current end-effector position, $\boldsymbol{x}_d$ is the desired position generated by the admittance controller (the position correction), and $\boldsymbol{x}_0$ is the desired equilibrium position (the target for the end-effector). $\boldsymbol{q}$ and $\boldsymbol{x}$ refer respectively to vectors in the joint space and the task space.

The transformations between them are achieved via forward kinematics (from $\boldsymbol{q}$ to $\boldsymbol{x}$) and inverse kinematics (from $\boldsymbol{x}$ to $\boldsymbol{q}$).

Position Control[6]

In position control, the robot aims to reach a predefined position using a PID controller. The controller calculates the error between the desired and the estimated position, then adjusts the actuator input to minimize this error. However, in environments shared with humans, this approach presents significant safety concerns. If an unexpected obstacle—such as a human limb—appears in the robot's trajectory, the controller will continue driving the robot toward its goal, potentially causing damage or injury, unless additional safety mechanisms are implemented.

Even when sensors are used to detect obstacles and modify the planned trajectory, the position control loop itself does not inherently respond to external forces. Therefore, in cases where a human pushes or resists the robot, the system would interpret this as an error and continue pushing in the opposite direction. This lack of compliance makes pure position control unsuitable for most pHRI scenarios.

Force Control Strategies[1]

Since physical contact is expected in pHRI, force control becomes more appropriate. It allows the robot to adapt its motion in real-time based on measured forces or torques at the interface with the human. Several force control strategies exist, notably: Hybrid, indirect and direct.

Hybrid Position/Force Control: [7][8]

In hybrid position/force control, each degree of freedom of the end-effector is assigned either to position control or to force control. These assignments are decoupled, assuming that task directions remain constant throughout the motion. The trajectory in each direction is handled either through a position controller or through a force controller. This separation assumes that the control axes are known in advance: the axes controlled in position and those controlled in force must be defined beforehand. In pHRI, the axes are dynamically changing during execution, which conflicts with the assumptions of hybrid control. This dynamic variability cannot be handled reliably by a controller that requires fixed, predefined task directions.

However, the use of a position controller raises the same issues discussed earlier. As a result, hybrid control is not well suited for physical human-robot interaction.

Direct Force Control [2]

Direct force controllers are controllers where there is a feedback loop for the force, giving a "direct" control over it, hence the name. They are typically used when precise control of the force at the end-effector is required. Although this level of precision would benefit from an accurate model of the environment, direct force control does not rely on dynamic modelling. Instead, it controls the applied force by minimizing the error between the measured force and the desired one.

However, this approach does not take into account the passivity or compliance of the robot. As a consequence, in the event of unexpected contact, the controller might issue commands that introduce excessive energy into the system, potentially resulting in unsafe or harmful interaction with the human user.

Indirect Force Control[8] Indirect force control modifies the position command in response to force measurements. In indirect control[8], the robot-environment interaction is modeled as a mass-spring-damper system, see Figure 2, allowing a combination of force and position control depending on the task and contact conditions. This approach is typically divided into two dual strategies: impedance control and admittance control. The dynamic model for a multi-degree-of-freedom (DOF) manipulator is given by:

$$M(\boldsymbol{q})\ddot{\boldsymbol{q}} + C(\boldsymbol{q}, \dot{\boldsymbol{q}})\dot{\boldsymbol{q}} + G(\boldsymbol{q}) + \tau_f = \tau + \tau_{ext}$$

where $\boldsymbol{q}$, $\dot{\boldsymbol{q}}$, and $\ddot{\boldsymbol{q}}$ represent the position, velocity, and acceleration vectors of the joints, respectively. $M(\boldsymbol{q})$ is the inertia matrix, $C(\boldsymbol{q}, \dot{\boldsymbol{q}})$ represents the Coriolis and centrifugal terms, $G(\boldsymbol{q})$ is the gravitational term, $\tau_f(\boldsymbol{q}, \dot{\boldsymbol{q}})$ the friction wrench[1],$\tau_{ext}(\boldsymbol{q}, \dot{\boldsymbol{q}})$ the external wrench from the environment, and τ the control torque. The link between the external torque $\tau_{ext}(\boldsymbol{q}, \dot{\boldsymbol{q}})$ and the external force is established through the Jacobian matrix J. This equation describes how the torque τ influences the movement of the manipulator by taking into account inertia, friction, and gravitational effects.

The control objective is to shape the dynamic behavior of the manipulator using the following desired dynamic model:

$$M_d(\ddot{\boldsymbol{x}} - \ddot{\boldsymbol{x}}_0) + D_d(\dot{\boldsymbol{x}} - \dot{\boldsymbol{x}}_0) + K_d(\boldsymbol{x} - \boldsymbol{x}_0) = F_{ext}$$

where M_d, D_d, and K_d are the desired inertia, damping, and stiffness matrices, and $\boldsymbol{x}$, $\dot{\boldsymbol{x}}$, $\ddot{\boldsymbol{x}}$ are the position, velocity, and acceleration vectors of the end-effector, respectively. $\boldsymbol{x}_0$ denotes the desired equilibrium position.

[1] Depending on the robot configuration the wrench can represent a force or a torque

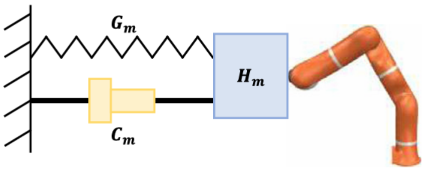

Figure 2: Model of a mass-spring-damper environment [9]

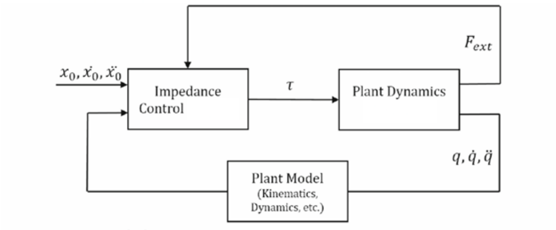

Figure 3: Impedance control block diagram [10]

- **Impedance control** treats the robot as a mechanical impedance and the environment as an admittance[7]. The robot reacts to position deviations by generating force outputs, which allows stable behavior during interaction with **stiff environments** by naturally absorbing disturbances and preventing large reaction forces. The block diagram shown in Figure 3 illustrates the feedback loop: position deviations are processed through the desired dynamic model to generate corrective torque commands that enforce a compliant and stable interaction. The impedance control law for a multi-DOF manipulator can be written as:

$$\tau_{imp} = MJ^{-1}\left(M_d^{-1}(F_{ext} - D_d(\dot{\boldsymbol{x}} - \dot{\boldsymbol{x}}_0) - K_d(\boldsymbol{x} - \boldsymbol{x}_0) + \ddot{\boldsymbol{x}}_0) - \dot{J}\dot{\boldsymbol{q}}\right) + C\dot{\boldsymbol{q}} + G + \tau_f$$

  where the output of the controller is a torque that is computed to eliminate the difference between the actual dynamics of the robot and the desired impedance model.

- **Admittance control** considers the robot as an admittance and the environment as an impedance[7]. It takes force inputs from the environment (e.g., from a human) and outputs motion commands. Admittance control is generally preferred for low-stiffness or free-space interactions due to its high positional accuracy and natural compliance[9]. It performs best with soft environments because the external forces are measured and directly fed into the admittance controller, which computes the desired motion vectors.

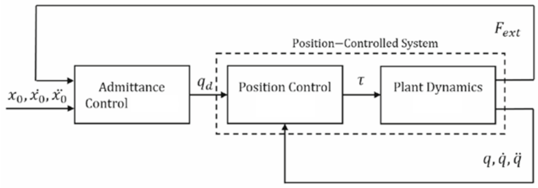

Figure 4: Admittance control block diagram [10]

These vectors are then provided to the position controller, which subsequently generates the reference torque commands for the robot, as shown in Figure 4.

For this controller, there are two equations to govern the system. The first is the admittance control law:

$$M_d(\ddot{\boldsymbol{x}}_d - \ddot{\boldsymbol{x}}_0) + D_d(\dot{\boldsymbol{x}}_d - \dot{\boldsymbol{x}}_0) + K_d(\boldsymbol{x}_d - \boldsymbol{x}_0) = F_{ext}$$

where M_d, D_d, and K_d are the desired inertia, damping, and stiffness matrices.In admittance control, $\boldsymbol{x}_d$ is continuously adapted in response to external forces, deviating from the reference trajectory $\boldsymbol{x}_0$ to provide a compliant motion. The robot then attempts to follow $\boldsymbol{x}_d$, not $\boldsymbol{x}_0$ directly.

This vector is then processed through a position controller, which outputs a control torque for the manipulator. The torque command is given by:

$$\tau_{adm} = K_p(\boldsymbol{q}_d - \boldsymbol{q}) + K_v\dot{\boldsymbol{q}} + C\dot{\boldsymbol{q}} + G + \tau_f$$

where K_v and K_p are the gains of the position controller.

Given its ability to naturally adapt to external forces and provide compliant motion, admittance control has become the most widely adopted strategy for physical human-robot interaction. This will be further discussed in the following section.

Admittance Control in pHRI[11][12][10][9][13][7] In the context of physical human-robot interaction, admittance control is the most widely used strategy, as it offers a natural response to human-applied forces. It prevents injuries caused by sudden robot movements or rigid trajectories by allowing the robot to yield and adapt to the user's motion in real time. This advantage stems from the direct measurement of external forces, enabling human contacts to be detected and handled immediately.

However, admittance control also presents some limitations, and there are situations where an impedance controller would be preferable. To overcome these issues,

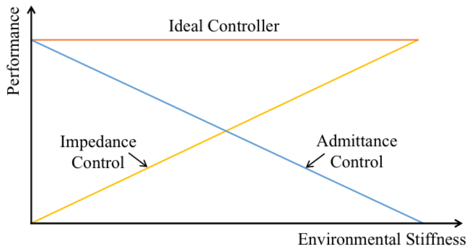

Figure 5: Performance of impedance and admittance controller depending on the stiffness if the environment[10]

some advanced applications combine both impedance and admittance strategies to leverage their respective advantages, as illustrated in Figure 5. This leads to the development of hybrid admittance-impedance controllers, capable of switching between behaviors depending on task demands or detected contact dynamics, thereby offering both stability and flexibility across diverse interaction scenarios.

Despite its limitations, admittance control is the most suitable strategy for the application of a robot assisting handwriting through cooperation with the user. This form of physical human-robot interaction requires the ability to sense the forces exerted by the user in order to adapt the robot's trajectory accordingly. Moreover, human interaction is typically characterized by soft and compliant behavior, which makes admittance control particularly well adapted to this context.

2.4 Existing Handwriting Assistance Robots

When reviewing the literature on handwriting-related robotics, several categories of systems can be identified. Some robots focus on mimicking human handwriting by reproducing character shapes, often without any interaction with a user. These robots have different architectures: Cartesian robots like the *AxiDraw*6a[14] or the *iDraw H*6b[15] and others such as the *Max Writer*6c[16] which uses a double parallel SCARA structure. A low-cost drawing robot was developed by [17]; its structure is a 5-bar linkage and it is controlled via a joystick. Some robots like the *Makelangelo Art Robot*6d[18] are designed to be used on a vertical plane, with a pen mounting system actuated by two cables linked to pulleys and weights. The height of the weights controls the position of the pen. Though their architectures differ, these robots all perform the same function: holding a pen over a sheet of paper and controlling its trajectory to write or draw.

Others rely on haptic devices that provide force feedback during writing tasks, sometimes for training or rehabilitation purposes. Examples include the *Geomagic*

*Touch*6e[19] a device used for drawing in 3D environments with force feedback to inform the user about contact within the virtual space, and the *Virtuose 3D Desktop*6f[20] which allows the user to co-manipulate a pen in 3D space. Even though it can guide the movement the maximal force that it can generate is only 3.3 N, that can be considered maybe to low for assisting handwriting. All those robot are shown in Figure 6

However, no robotic systems have been specifically designed to assist users in real-time handwriting tasks through physical cooperation. The closest related application can be found in upper limb rehabilitation robots, which will be discussed in the next subsection. These cooperative systems are not intended to replace human movement, but rather to guide or support it—making them particularly relevant in contexts such as motor skill learning or rehabilitation.

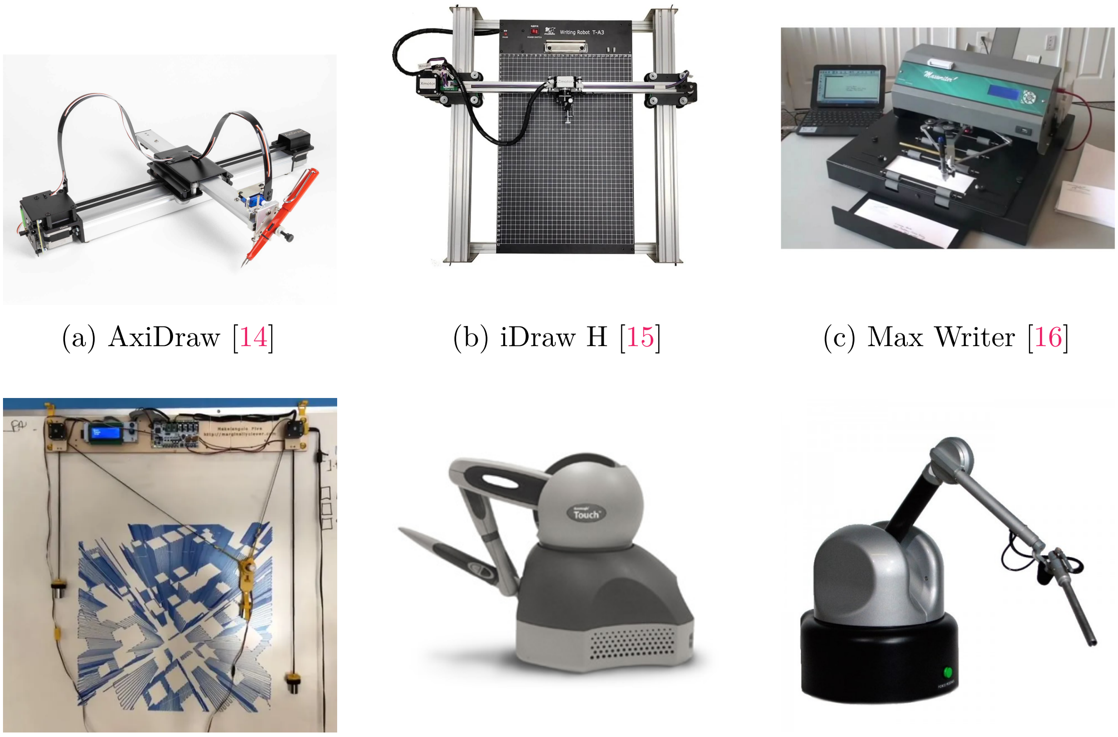

(a) AxiDraw [14] (b) iDraw H [15] (c) Max Writer [16]

(d) Makelangelo [18] (e) Geomagic Touch [19] (f) Virtuose 3D [20]

Figure 6: Examples of handwriting-related robotic systems and haptic devices.

2.5 Robots for Upper Limb Rehabilitation

Several robotic systems for upper limb rehabilitation already exist on the market, and unlike the previously discussed handwriting robots, these systems are designed to interact continuously with the user. They are therefore more relevant to the approach presented in this work. Robots such as the REAplan, MIT-MANUS, ARMASSIST, SY-UEA2, and Arméo Power, shown in Figure 7, are used for the rehabilitation and reeducation of upper limb movements following neurological injuries such as stroke.

REAplan[21] is a planar Cartesian rehabilitation robot that assists patients in recovering arm mobility by providing either assistance or resistance during guided movements in a horizontal plane. The patient holds a handle attached to the robot and performs exercises, often structured as games, that stimulate voluntary arm movements. The system is designed to adapt its behavior based on the patient's force input, supporting active engagement.

MIT-MANUS[22] is also a planar rehabilitation robot originally developed at MIT, where the patient also holds a handle to interact with the robot. It can provide passive guidance when the patient cannot initiate movement, or adaptive assistance when movement is detected. The robot's assistance adapts to the user's needs and level of engagement in the exercise. Unlike the REAplan, it uses a parallel robotic structure rather than a classical Cartesian configuration.

ARMASSIST[23] is a low-cost, portable robotic system targeting shoulder and elbow rehabilitation. Unlike REAplan, ARMASSIST is not limited to planar movement. As with the two previous robots, the patient holds a handle, but here a forearm support is added. It facilitates active, gravity-compensated arm movements and measures parameters such as arm orientation and lifting force. It does not guide the arm directly, but reduces the physical effort required to perform movements. The system includes training games to enhance patient engagement.

SY-UEA2[24] is a mobile-based robot equipped with optical sensors. It is also designed for upper limb rehabilitation and, like the previous systems, integrates gamification to enhance user motivation. It also features a handle and forearm support for the interaction. It aims to deliver affordable therapy while maintaining user engagement through interactive tasks.

Arméo Power[25] is a fully actuated exoskeleton for three-dimensional upper limb rehabilitation. It is self-supporting and attaches to the patient's entire arm, providing motorized assistance at the shoulder, elbow, and wrist joints. Unlike table-based systems, Arméo Power enables functional training in the full workspace of the arm.

Some features are common to all these robots, such as exercises presented in the form of games to increase user involvement, and adaptive levels of assistance based on user performance. However, their mechanical structures vary: from Cartesian planar robots to mobile-base systems, parallel mechanisms, and even full upper-limb exoskeletons.

(a) REAplan[21]

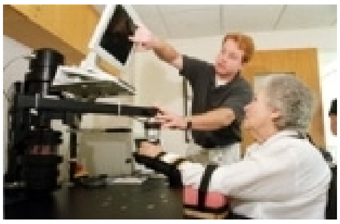

(b) MIT-MANUS[22]

(c) ARMASSIST[23]

(d) SY-UEA2[24]

(e) Arméo Power[25]

Figure 7: Examples of upper limb rehabilitation robots.

2.6 Design method

In this work, the design methodology followed is the one proposed in the course LMECA2801 Machine Design. This method, also known as the Pahl and Beitz approach, is particularly well-suited to engineering design processes, which are often ill-defined at the beginning and become progressively clearer as the design evolves. It combines rigor with the flexibility needed to handle the inherent uncertainty of complex projects. The method consists of four main stages: (1) clarify the needs and express them in terms of functions, (2) search for concepts and possible solution ideas, (3) evaluate the proposed solutions based on defined criteria and select the most suitable one, and (4) develop the chosen concept in more detail, including detailed drawings and virtual prototyping.

3 Specification Sheet

3.1 Introduction

In every design process, the specification sheet is the first step. It is essential to understand the needs, limitations, and constraints in order to develop the best possible solutions. It defines the boundaries within which the work must be carried out. For this project, it will start with the problem we are trying to address. This will then be translated into functions and constraints, summarized in a table. Each function and constraint will be detailed, along with the reasons for their inclusion and the methods by which the values were established. This will conclude the section.

3.2 Needs and Context Description

Nowadays, between 10 and 15% of children are affected by dyslexia. Dyslexia is defined by Lyon et al. [26] as a specific learning disability of neurobiological origin, characterized by difficulties in accurate and/or fluent word recognition. It is manifested by persistent spelling difficulties [27], which can occur at three levels:

- *Sublexical level:* letters are added, omitted, or incorrectly reproduced within words.
- *Lexical level:* words are spelled incorrectly due to poor memorization of their orthographic forms.
- *Grammatical level:* verbs, plurals, and other grammatical agreements are not properly applied.

Despite its importance, handwriting development in children with dyslexia has been comparatively less studied, even though at least 50% of children with dyslexia exhibit handwriting difficulties [28], including slowness, poor legibility, and signs of developmental coordination disorder. To better understand the nature of handwriting difficulties in dyslexia, researchers have investigated the bidirectional influence between spelling and handwriting in both dyslexic and non-dyslexic children.

Studies on the influence of spelling on handwriting [29] show that children with dyslexia make more spelling mistakes even during copying tasks, and they tend to increase the number of gaze lifts. Moreover, the complexity of word spelling significantly impacts their writing speed and gaze behaviour.

Conversely, studies on the influence of handwriting on spelling [30] highlight that several graphical characteristics of words, such as modified links, angles, curves,

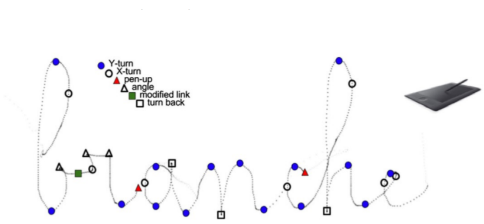

(a) Graphical characteristics that influence handwriting and create difficulties in children with dyslexia.[31]

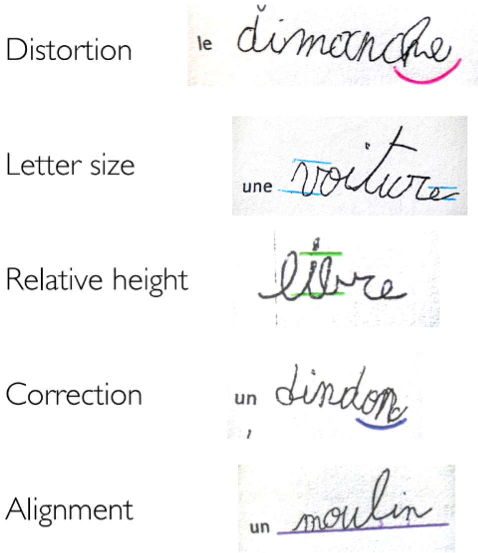

(b) Handwriting quality of children with dyslexia.[31]

Figure 8

pen-ups, and overall word length, as shown in Figure 8a, can lead to handwriting difficulties, as illustrated in Figure 8b.

These findings raise two key questions: do children with dyslexia have a specific handwriting deficit, and are their handwriting difficulties solely the result of spelling deficits? Investigations have shown that children with dyslexia are more sensitive to graphic complexity, and that their handwriting difficulties cannot be fully explained by spelling issues alone. When writing, they exhibit slower movements, more pauses, and a higher error rate.

Gosse et al. [32] examined graphomotor dysfunction in children with dyslexia and reported reduced activation in the neural network associated with handwriting. Additionally, Van Reybroeck M. et al. [33] implemented a finger-writing intervention and observed improvements in reading, spelling, and handwriting, demonstrating that finger motion helps children develop motor patterns for letter formation.

These insights directly motivated the idea of developing a handwriting-assisting robot. The robot aims to co-manipulate the pen with the child and support the creation of motor patterns necessary for letter formation. In simple terms, the objective is to help children automate the basic motor sequences involved in writing, freeing cognitive resources for higher-level tasks such as spelling and composition.

To elaborate on the needs: as stated above, the robot should be capable of co-manipulating a pen with a child and operating through different modes. The first mode would guide the child's hand movements, helping them create the necessary motor patterns. The second mode would be a transparent mode, where the robot is guided by the user; it monitors the child's handwriting and can intervene to correct the trajectory by taking partial control if necessary.

From an engineering perspective, these two modes can be seen as a master/slave dynamic, where the robot either leads (master) or follows (slave) the child's movements. Additionally, the level of guidance provided by the robot should be adjustable to adapt to the child's progress. The pen's position should also be selectable, and a visual display could be added to help the child visualize the intended movement or receive additional instructions. This overall set of capabilities defines what the robot must be able to achieve. Based on these needs, a formal specification can now be established, which will be developed in the next subsection.

3.3 Functional and Technical Requirements

Now that the context has been established and the user needs have been expressed, it is time to formalize a specification sheet. This consists in translating the functional expectations into main functions and main constraints for the design of the robot. This step constitutes the foundation of any structured design process.

Three main functions(MF) have been identified: *Handwriting assistance*, *Safety* and *Pen orientation*. Each of these includes several sub-functions, or criteria, derived from the user's expectations and the operational context. Likewise, a set of constraints has been defined, including *Environment*, *Ergonomics and usability*, and an optional but valuable constraint: *Visual feedback*. Each constraint is also broken down into relevant sub-elements.

The purpose of Table1 is to summarize, in a clear and concise format, the complete set of requirements that will guide the subsequent design phases. Each element presented in the table will be detailed in the following subsection.

Context: Robotic design – Design and prototyping of a robot for assisting handwriting		
Date	**Origin**	**Main Function**
28/10/24	Perilleux A.	1. Assist handwriting
28/10/24	Perilleux A.	2. Safety
28/10/24	Perilleux A.	3. Pen handling
		Criteria and levels of MF
28/10/24	Perilleux A.	1.1 Transparency mode
27/01/25	Perilleux A.	1.2 Guiding / Assisted mode
28/10/24	Perilleux A.	1.3 Adjustable level of guidance
28/10/24	Perilleux A.	1.4 Accuracy 0.15 mm
28/10/24	Perilleux A.	1.5 Maximum force 110 N
28/10/24	Perilleux A.	1.6 Speed range 0–120 mm/s
28/10/24	Perilleux A.	1.7 Acceleration range 0–2000 mm/s^2
27/01/25	Perilleux A.	1.8 Allow the user to see their writing
05/11/24	Perilleux A.	1.9 Detect contact with paper (Z-axis: writing or in-air)
05/11/24	Perilleux A.	1.10 Maintain paper on the support
24/11/24	Perilleux A.	1.11 Workspace: A4 + 10% (231 x 326.7 mm^2)
28/10/24	Perilleux A.	2.1 No collision
28/10/24	Perilleux A.	2.2 Motion allowed only when the pen is held
27/11/24	Perilleux A.	2.3 ISO/TS 15066:2016
05/11/24	Perilleux A.	2.4 Maximum noise level [dB] (ISO 3740)
05/11/24	Perilleux A.	2.6 IP rating: IP44
28/10/24	Perilleux A.	3.1 Ambidextrous
28/10/24	Perilleux A.	3.2 Adjustable before use
28/10/24	Perilleux A.	3.3 Fixed during use
28/10/24	Perilleux A.	3.4 Able to write on paper
		Constraint functions
28/10/24	Perilleux A.	4. Ergonomics and usability
28/10/24	Perilleux A.	5. Environment
05/11/24	Perilleux A.	6. Visual support and feedback(Optional)
		Criteria and levels of constraint functions
28/10/24	Perilleux A.	4.1 Device must be placed on a table
28/10/24	Perilleux A.	4.2 For children aged 5 to 10
28/10/24	Perilleux A.	4.3 Friendly design to avoid fear
28/10/24	Perilleux A.	4.4 Pen suitable for a child's hand
28/10/24	Perilleux A.	5.1 Electrical supply: 220 V / 50 Hz
28/10/24	Perilleux A.	5.2 Connectivity with a computer

Table 1: Summary of functional and constraint requirements

3.4 Detailed Description of Functions and Constraints

Assisting Hand writing the first main function, *Assisting hand writing* is the one with the most sub-function, as it is the core of the robot application. it constraint 11 criteria that are going to be developed here:

- **MF 1.1 and 1.2:** The core idea of the robot is its assistance in hand writing to do so two mode are needed, transparent and guiding. In transparency mode, as the name state, the robot should not oppose resistance to the user movement, the robot should be passive the user is the one doing all the movement. Nonetheless, during transparency mode the robot is still recording the position of the end-effector to make sure the movement. In guiding mode the robot initiate the movement it is in control, there the robot is active.

- **MF 1.3** The level of guidance of the robot during the guiding mode should be adjustable to suit the user needs and progress. The guidance level can be defined in terms force threshold or trajectory deviation from a reference.
- **MF 1.4** The required positioning accuracy of the robot is set to approximately 0.15 mm, corresponding to 5% of the average handwritten letter height. The 5% value was not derived from measurements but was deliberately chosen as a fixed design criterion. Based on this assumption, and considering an average letter height of approximately 3 mm -estimated from handwriting learning workbooks and the dataset provided by Prof. Van Reybroeck—an accuracy target of 0.15 mm was established. The detailed data analysis supporting this assumption is presented in the next subsection. While letter sizes and line spacing may vary across countries and educational contexts, 3 mm was adopted as a representative average for specification purposes.
- **MF 1.5** The robot must not exert a guiding force greater than the maximum resistance a child could oppose. Since no direct data exist on the forces applied during handwriting by children, an upper limit was estimated using internal and external shoulder rotation strength as a conservative reference. The posture used for these measurements—arm aligned along the body with the forearm forming a 90° angle—is used as an approximation of the arm position during writing. Data from McKay et al. [34], based on 1,000 individuals aged 3 to 101, were used. The average maximum force for shoulder rotation in boys aged 3–9 was 56.1 N, with a standard deviation of 27.1 N. To cover 95% of this population, the limit was set at 110 N by adding two standard deviations. Although the robot is intended for both boys and girls aged 5–10, the higher male values were retained to ensure safety in all use cases.
- **MF 1.6** The robot must be able to operate reliably within a velocity range of 0 to 120 mm/s. This operational range was determined from handwriting trajectory data collected and analyzed by Prof. Van Reybroeck. The corresponding analysis is presented in the next section.
- **MF 1.7** The robot must also be able to function within an acceleration range of 0 to 2 m/s^2, to reflect the dynamics of typical handwriting movements. As with speed, this range was extracted from the same dataset, and the analysis is detailed in the following section.

- **MF 1.8** During operation, the user must have a clear and unobstructed view of the pen tip, the writing surface, and the resulting trace. The robot design must not visually block or interfere with the user's natural field of vision while writing.
- **MF 1.9** The robot must be able to passively detect when the pen is in contact with the paper. This information is not used to modify the control in real-time but is essential for interpreting the recorded data. It enables the identification of writing phases (e.g., tracing a letter, placing a dot on an "i") versus non-writing transitions (e.g., moving to a new word, returning to a new line).
- **MF 1.10** The paper must remain still in place on the robot's support surface during the entire operation. Any unwanted movement of the sheet could compromise the precision of handwriting assistance and data interpretation.
- **MF 1.11** The robot's workspace must be at least 20% larger than the surface area of a standard A4 sheet, while maintaining the same aspect ratio. This corresponds to approximate dimensions of at least 231 mm x 326.7 mm. This additional area was deliberately chosen to provide a margin for manual placement of the sheet and to ensure that the entire writing surface remains accessible during operation.

Safety As highlighted in the state of the art, safety is a major concern in human–robot interaction. This is particularly critical in the present context, as the targeted users are young children aged 5 to 10. The second main function therefore focuses on all the safety requirements that must be met by the system.

- **MF 2.1** The only physical contact between the robot and the user must occur through the pen, which serves as the designated interface for interaction. No other part of the robot shall come into contact with the user during operation. This constraint ensures predictable and controlled interaction, and reduces the risk of unintended contact, especially given that the users are children aged 5 to 10 years.
- **MF 2.2** The robot must only initiate movement when physical contact between the user and the pen is detected. This simple condition prevents the robot from moving when the user is not engaged with the device, such as when the pen is dropped or laid aside, thereby improving safety and reducing the risk of unwanted or surprising motion.
- **MF 2.3** The robot should follow the guidelines defined in ISO/TS 15066:2016, which provides safety limits and risk assessment methods for physical hu-

man–robot interaction. These guidelines are intended to ensure that all contact remains within safe thresholds, enabling safe collaboration between humans and robots.

- **MF 2.4** The robot must comply with the maximum permissible noise level defined by ISO 3740. During operation, the sound pressure level must not exceed 55 dB, to ensure an environment that is safe and comfortable for children aged 5 to 10. Limiting noise exposure is essential to avoid stress, distraction, or discomfort for young users.
- **MF 2.6** The robot must meet an IP44 rating in accordance with the IEC 60529 standard. This ensures protection against solid objects larger than 1 mm and splashing water from any direction. Given that the robot is intended for use in offices or educational settings, this level of ingress protection helps ensure both durability and safe operation in environments where dust or accidental spills may occur.

Pen handling The pen is a central component of the device, as it serves both as the physical interface between the user and the robot and as the element responsible for producing the handwriting.

- **MF 3.1** The robot must be suitable for both right- and left-handed users.
- **MF 3.2** The position and orientation of the pen must be adjustable prior to use so that the user can place it in a comfortable configuration.
- **MF 3.3** During operation, the pen must remain fixed in the selected position. The robot's guidance concerns the motor patterns required to form letters and words, not the fine movements produced at the hand level.

Ergonomics and usability This group of constraints addresses how the robot is physically handled, perceived, and used by the child. It includes aspects related to safety, ease of use, and visual design to ensure a comfortable and non-intimidating interaction.

- **CF 4.1** The robot must be designed to rest on a standard office desk. While no strict size or weight limits are defined at this stage, its dimensions and mass must remain compatible with stable tabletop installation and typical classroom or office environments.
- **CF 4.2** Since the users are children aged 5 to 10, the robot must be free of sharp edges and must prevent access to any moving or sensitive parts. Children are naturally curious and tend to touch anything within reach;

therefore, the robot must be designed in such a way that no dangerous areas are accessible during normal use.

- **CF 4.3** Additionaly the young age of the user should encourage the visual design of the robot to be as friendly as possible to not affraied or stress them, the robot is not their to be seen as someting scary the child should be interacting with it naturaly.
- **CF 4.4** The pen must be appropriately sized for a child's hand. It should not be too large or heavy, in order to allow a comfortable grip and ease of use for users aged 5 to 10.

Environment The robot is intended to operate in a standard indoor environment such as an office or classroom. Accordingly, it must be compatible with typical electrical infrastructure and support basic connectivity features to facilitate data exchange and task updates.

- **CF 5.1** The robot must be compatible with a standard electrical supply of 220 V at 50 Hz, as typically found in offices and schools.
- **CF 5.2** The robot must support connectivity with external devices in order to export usage data and import new exercises or control routines.

Visual support and feedback The possibility to add a visual support to offer guidance and feedback to the user should be possible.

3.5 Analysis and Justification of Key Specifications

Context The data used in this analysis were provided by Prof. Van Reybroeck and originate from a previous study published in one of her papers [31]. These data are relevant for the present work as they represent handwriting movements performed by children whose age corresponds to the target users of the robot. The complete data collection procedure is described in the original publication; the essential elements are summarized below.

Participants were second-grade children from a regular primary school in the French-speaking region of Belgium. All children were typically developing and had no reported language or learning disorders such as dyslexia. One child was excluded from the final dataset for scoring more than two standard deviations below the norm on several control tasks, resulting in a final sample of 19 children (mean age: 7.75 years, SD = 0.22; 10 boys).

The recordings took place in an empty classroom over a three-week period and were conducted by the same experimenter. Control tasks were administered individually in 30-minute sessions, except for the standardized spelling task, which was completed in class. The experimental handwriting task was carried out in groups of four children, assisted by the experimenter and an engineer, and lasted approximately 30 minutes.

Each child used a Wacom Intuos Pro Medium digital tablet with a Wacom Inking Pen. The tablet measured $380 \times 251 \times 12$ mm, with an active area of 224×140 mm. A standard A4 paper sheet was taped over the tablet to replicate usual writing conditions. The boundaries of the active area were outlined on the paper to guide the children.

Children were asked to write down words they heard during a dictation task, at their natural writing speed. No instructions regarding performance or writing quality were given, and they were informed that the task was unrelated to school assessment. Moreover, they were not told that the quality of their handwriting would be analyzed. The handwriting trajectories were recorded in real time at a sampling interval of 7–8 ms.

These data provide a reliable reference for typical handwriting behavior in the target age group and are therefore valuable for defining realistic specifications for the robot's motion capabilities.

Data Format and Pre-processing The data of 4 recording were provided in Excel spreadsheets where several parameters were recorded for each time sample. These include: *packet time* (in milliseconds), *serial packet number* (unitless incremental counter), *X, Y, Z positions* (in pixels), *normal pressure* (in arbitrary units ranging from 0 to 1023), *azimuth* (in degrees, 0–360), and *altitude* (in degrees, 0–90).

The *packet time* corresponds to the absolute timestamp of each recorded sample. The *serial packet* is an incremental counter that can be used to verify the recording order. The X and Y values represent the 2D coordinates of the pen tip on the tablet's surface, while Z indicates the vertical distance of the pen from the tablet. The *normal pressure* gives an estimate of the force applied by the pen on the surface. The *azimuth* is the angle between the projection of the pen in the X–Y plane and a reference axis (typically the X-axis). The *altitude* is the angle between the pen and the surface of the tablet, where 90° corresponds to a vertical position.

For this work, only the X and Y positions and the packet time were used to compute the pen trajectory, speed, acceleration, and letter size. The normal pressure was also retained to distinguish between writing phases (pen in contact with the paper) and non-writing movements (pen hovering or switching lines). The Z position, azimuth, and altitude were discarded, as they are not relevant for the current analysis.

To convert position data from pixels to millimeters, a conversion factor was computed using the tablet's resolution, which is 5080 dpi (dots per inch). Given that 1 inch = 25.4 mm, the resulting conversion factor is approximately 0.005 mm/dot. Likewise, as packet times were provided in absolute milliseconds, time differences between samples were calculated to enable the computation of velocities and accelerations.

Processing The first observation from the raw data is that the time interval between successive samples fluctuates between 7 ms and 8 ms, with occasional longer gaps likely due to irregularities in data acquisition. To ensure a consistent sampling frequency and enable accurate numerical differentiation, the data were resampled at 125 Hz following a first-order linear interpolation of the X and Y coordinates with respect to time. The choice of 125 Hz was made because it closely matches the original sampling frequency of the recordings.

After resampling, the position signals were filtered using a zero-phase fourth-order Butterworth low-pass filter implemented via the `filtfilt` method, in order to remove high-frequency noise. A zero-phase method applies the filter in both forward and backward directions, cancelling phase distortion and preserving the temporal structure of the signal. A comparison of the raw and resampled position signals is shown in Figure 9a. The similarity between the curves confirms that the signal structure was preserved. Figure 10 further illustrates the spatial coherence of the data by reconstructing the pen trajectory during a writing session. The straight segments observed between certain letters are due to gaps in pen detection when the pen was lifted too far from the tablet surface, resulting in discontinuities and sudden position jumps.

Velocities were then computed as the first derivative of the filtered positions using the `numpy.gradient` function, and subsequently filtered using the same Butterworth configuration to suppress noise introduced during differentiation.The `numpy.gradient` function was chosen over a simple finite difference method (e.g., $\frac{\Delta x}{\Delta t}$) because it provides a more accurate and stable numerical derivative by using central differences in the interior and first differences at the boundaries, thus reducing the impact of noise and edge artifacts. Figure 9b shows a zoomed comparison of the velocity signals. The resampled signals appear smoother than the raw ones, while preserving their overall shape.

For acceleration, a second-order Butterworth filter was preferred, as the fourth-order version caused excessive attenuation of signal amplitude, potentially masking

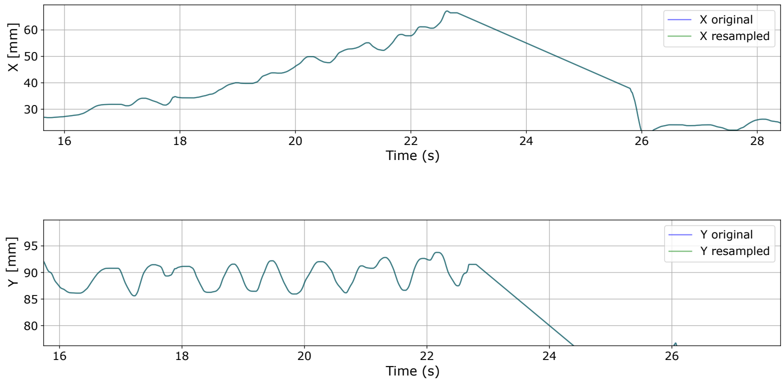

(a) X and Y position comparison between raw data and resampled data.

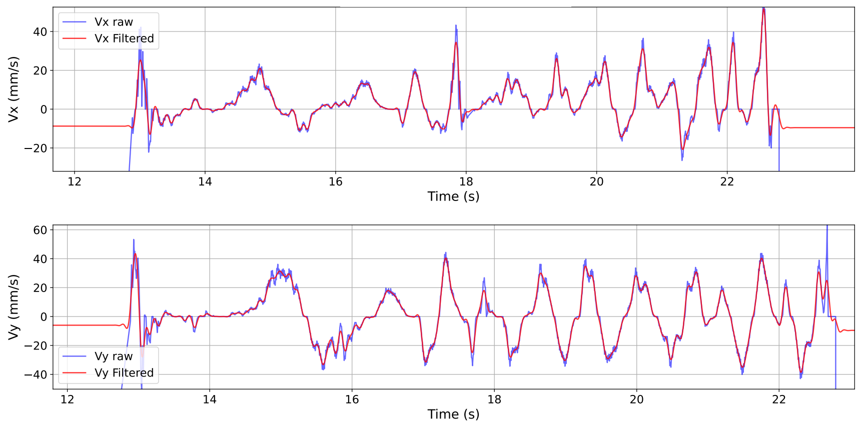

(b) Velocity comparison between raw data and resampled data.

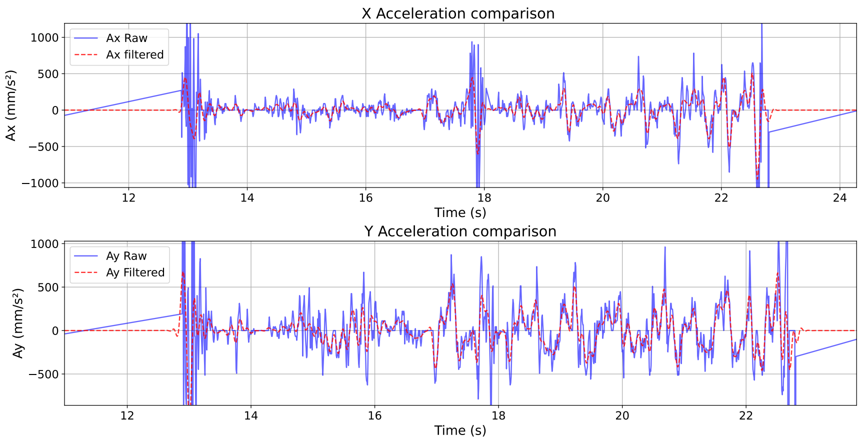

(c) Acceleration comparison between raw data and resampled data.

Figure 9

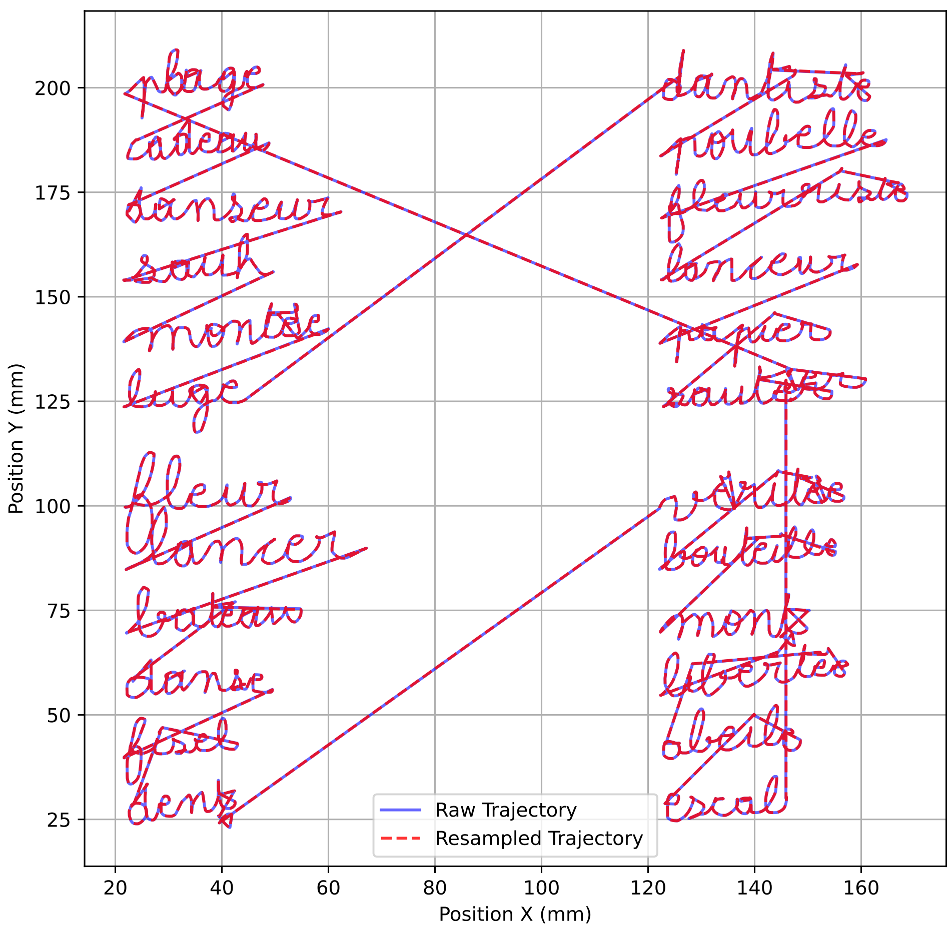

Figure 10: Trajectory comparison between raw data and resampled data.

important dynamic features. Acceleration signals showed more pronounced differences between raw and resampled data, as illustrated in Figure 9c. The raw data exhibit more fluctuation due to sampling noise and the sensitivity of acceleration to signal irregularities. Although the differences between the raw and resampled acceleration signals are more pronounced than those observed for velocity, they remain moderate. The overall shape and key extrema of the signal are preserved, confirming the validity of the preprocessing.

In addition to resampling, the intervals during which the pen was in contact with the writing surface—identified via the *NormalPressure* signal—were mapped onto the resampled dataset. Preserving these intervals is essential for isolating active writing phases from pen movements in the air, which do not require motor assistance.

Once the data were processed, the maximum values of velocity and acceleration, as well as the average letter size, were extracted. To estimate the maxima, absolute values of the velocity and acceleration signals were computed, and the mean plus three standard deviations was taken as a robust upper bound, excluding extreme outliers. This procedure was repeated for four recordings, and the highest values were retained. The maximum velocity was found to be 0.12 m/s, and the maximum acceleration was $2\,\mathrm{m/s^2}$.

Letter height was estimated manually by inspecting the position plots. Since the words written by the children were not aligned on perfectly straight baselines, automatic detection was not implemented. However, visual inspection allowed for reliable measurements. Letter sizes ranged from approximately 2 mm to 5 mm, with an average around 3 mm.

These results provide a solid empirical basis for defining key specifications of the robot in terms of movement dynamics and spatial precision. More detailed and unzoomed visual representations of all recordings and signals are provided in Appendix 1 for reference and transparency.

3.6 Conclusion of the Specification Sheet

The specification sheet defines both the scope of the project and the essential guidelines for the subsequent design phase. The key specifications include the two modes of operation—transparency and guidance—the maximum allowable force of 110 N, a velocity range of 0 to 0.12 m/s, an acceleration range of 0 to $2\,\mathrm{m/s^2}$, and a positioning accuracy of 0.15 mm. Additionally, the co-manipulation of the pen, which serves as the physical interface between the user and the robot, remains central to the concept. These criteria will serve as the foundation for the upcoming design choices.

4 Design Methods

4.1 Kinematic structure

Now that the specification sheet is established the next step is the start the design of the solution to the problem according the specification. To do so several design methodologies exist. The method followed in this work, as state in the state of the art, is the one taught in the course LMECA2801 – Machine Design. At this point the first step has been done and the second and third step can be subdivided into five smaller step.

1. Identify all the functions required for the machine.
2. Generate possible solutions.
3. Break down each solution to associate specific parts with specific functions and compile all possible solutions for each function in a morphological table.
4. Create concept variants by assembling coherent sets of solutions.
5. Evaluate the concept variants using weighted criteria.

Although this work generally follows the expected methodology, some liberties were taken. The design process was carried out in two steps: first the kinematic structure was defined, followed by the rest of the system. This choice was made to ease the design process, as some initial difficulties were encountered in determining how to begin. Once the kinematic structure was selected, the remainder of the solution was developed accordingly.

Before analyzing the different robot architectures, it is important to state a key design decision that significantly influences the selection: the Z axis will remain passive (i.e., non-actuated). As a result, only planar robot structures are considered in this study. This is a choice to ease the design and limit the actuation because the movement in the Z axis are relatively small around 2 cm.this movement will remain free and made by the user.

Description of the different structure To achieve to motion in the X-Y plane at two degree of freedom are needed, several cinematic structure are capable of achieving it. Here are the five planar structure:

- **SCARA:** The SCARA structure is composed of two revolute joints in series. The axes of rotation are parallel to each other and oriented perpendicular to the XY-plane.

- **Cartesian:** The Cartesian structure consists of two prismatic joints in series and orthogonal to each other. One joint provides motion along the X-axis, and the other along the Y-axis.
- **Cylindrical:** The cylindrical structure includes a revolute joint followed by a prismatic joint. The revolute joint's axis is perpendicular to the XY-plane, while the prismatic joint enables translation in the XY-plane.
- **Delta:** The Delta structure consists of three identical arms, each composed of two revolute joints. The first joint of each arm is fixed to the base and is typically actuated, while the second joint is passive and part of a parallelogram linkage that ensures the orientation of the end-effector. All three arms are connected to a common mobile platform, forming a closed-loop kinematic chain. It is a parallel structure, in contrast with the three previously described serial architectures.
- **Parallel SCARA:** The parallel SCARA consists of two SCARA-type arms connected at the end-effector. Each arm includes two revolute joints, but only the first joint of each arm is actuated. All rotation axes are parallel to each other and oriented perpendicular to the XY-plane. This closed-loop configuration allows for planar motion while reducing the number of actuators compared to the serial SCARA.

One might wonder why anthropomorphic and spherical robots are not included in the comparison. These architectures are intrinsically designed to operate in three-dimensional space. Although it is theoretically possible to constrain their workspace to a 2D plane, they retain unnecessary degrees of freedom for the task at hand. In contrast, the other structures considered can naturally operate in a plane or can be easily modified (e.g., by removing a joint) to restrict their motion to 2D. Using a robot with inherently 3D kinematics for a planar co-manipulation task would introduce unnecessary complexity in control and may raise safety concerns. The Delta robot is still included in the comparison, although it is also intrinsically a 3D structure. However, its parallel architecture offers specific advantages—particularly in terms of low moving mass and dynamic performance—that make it worth evaluating in the context of this application.

Criteria and evaluation The criteria used to evaluate the different structures listed above are: the A4-to-workspace ratio, dynamic performance (inertia), precision, complexity, and workspace clutter. Before presenting the comparative table, each criterion is described in detail, along with the weighting factors assigned to them.

These weights reflect the relative importance of each criterion in the context of

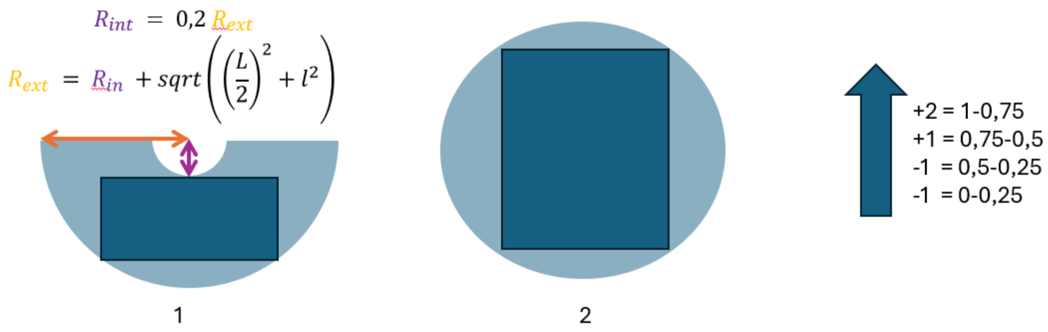

Figure 11: Area ratio: A4 + 20% in dark blue; workspace in light blue; 1 for SCARA, parallel SCARA and cylindrical; 2 for Delta; and the scale for grading

this specific application. There is no universal rule for assigning such weights; their values are determined according to the priorities and constraints of the task at hand.

- **Ratio A4 / Workspace** Robot workspaces are not always exactly what is required and can sometimes exceed the necessary area. A workspace larger than required means that the end-effector may reach positions outside the target zone, potentially causing collisions with the environment or the user. In this case, the desired workspace is a rectangle measuring 231 mm × 326 mm. For the Cartesian structure, the workspace can match this rectangular shape exactly. For the SCARA, cylindrical, and parallel SCARA structures, the workspace was approximated by half a circle—the smallest one in which the desired workspace could fit. A smaller circle, with a radius equal to 20% of the larger circle's radius, was subtracted to represent the robot base area, which cannot be reached by the end-effector. Figure 11 shows the different areas and the scale used to determine the marks in the evaluation table. The ratio between the two areas was computed and is given in Table 2.

Structure	**Workspace** [mm^2]	**A4 + 20% / Workspace**	**Marks**
SCARA	189421	0.399	-1
SCARA //	189421	0.399	-1
Cartesian	75794	1.000	+2
Cylindrical	189421	0.399	-1
Delta	252532	0.299	-1

Table 2: Ratio A4/workspace comparison table

- **Dynamic (Inertia)** This criterion represents the mass that each structure must move in order to actuate the end-effector. At this stage, no precise mass values are available for the robot, so this remains a qualitative criterion. Nonetheless, it is evident that some robots require more mass to be moved—typically the case for serial robots. Parallel robots have the advantage of moving less mass. A major contributor to the moving mass is the weight of the motors, and parallel robots benefit from having stationary motors. While the rest of the structure can be made as light as possible, motors cannot. Greater mass results in higher inertia, which can lead to more severe consequences in the event of contact.

- **Complexity** To evaluate complexity, the minimum number of motors, joints, and guiding elements required to build the robot was considered, summed, and normalized. These values are presented in Table 3. The resulting scores were used in the evaluation table. The same grading scale as for the A4/workspace ratio (shown in Figure 11) was applied.

Structure	Joint Count	Motor Count	Passive Joints	Total Parts	A4 Coverage Ratio	Z-score
SCARA	2	2	0	4	1.0	2
Parallel SCARA	2	4	2	8	0.5	0
Cartesian	2	2	2	6	0.67	1
Delta	3	6	0	9	0.44	-1
Cylindrical	2	2	1	5	0.8	2

Table 3: Comparison of complexity based on the number of motors, joints, and guiding elements across different kinematic structures

- **Precision** As with the dynamic criterion, this one also highlights the advantage of parallel structures, which tend to offer greater precision than serial ones.
- **Clutter Compared to the Workspace** The problem to be solved is strictly planar (2D). Therefore, some robots are more suitable for this task in terms of the volume they occupy. This criterion highlights the fact that the Delta robot is the only non-planar structure, and therefore occupies significantly more space. Even though no maximum volume was specified in the design requirements, the robot must be installed on a table. This is mainly a criterion used to point out a drawback of the Delta.

Criteria weighting The weights assigned to the criteria are normalized such that their sum equals 1. The first two criteria relate to safety, which is the most critical aspect when designing a collaborative robot; hence, each was assigned a weight of 0.25, together accounting for half of the total. Precision was assigned a weight of 0.3, as it is crucial in this project—the average size of a handwritten letter being approximately 3 mm. For complexity, it is worth recalling that the more complex a mechanical system is, the greater the likelihood of failure. This criterion was assigned a weight of 0.2. Lastly, clutter relative to the workspace, which serves mainly to highlight a specific drawback of the Delta robot, was given a weight of just 0.05.

Structure Choice Based on the explained and weighted criteria, Table 4 summarizes the evaluation. The structure that emerges as the most suitable according to these criteria is the Cartesian architecture.

Criteria	Weight	1 // SCARA	2 SCARA	3 Cartesian	4 Delta	5 Cylindrical
A4 / Workspace Ratio	0.225	-1	-1	2	-1	-1
Dynamic (Inertia)	0.225	1	-1	-1	1	-1
Precision	0.300	1	0	0	1	0
Complexity	0.200	0	2	1	-1	2
Clutter / Workspace	0.050	0	0	0	-1	0
Total Score	**1.000**	**0.30**	**-0.05**	**0.425**	**0.05**	**-0.05**

Table 4: Multicriteria evaluation of candidate kinematic structures

4.2 Function identification

Now that the kinematic structure has been selected, attention must be turned to the functional decomposition of the robot. A set of eight essential functions has been identified to comprehensively represent the robot's operational and structural requirements. These functions are listed below, each accompanied by a brief, solution-independent description:

- **Active translation transmission:** Enable the transmission of torque and linear motion from the actuator to the moving element.
- **Motorisation:** Provide actuation for the active translational movement.
- **Maintaining the robot's position on the tabletop:** Ensure stable positioning of the robot relative to the working surface.
- **Structure layout:** Define the overall configuration and spatial arrangement of the structural elements.
- **Materials:** Satisfy structural, mechanical, and environmental constraints through appropriate material selection.
- **Adjustable pen orientation:** Ensure the writing instrument can be positioned with the desired orientation and held in place
- **Pen holder:** Provide mechanical support and integration for the writing instrument.
- **Passive Z-axis translation:** Permit vertical displacement in accordance with the writing surface or task-specific requirements.

4.3 Morphological table

With the functional breakdown established, the morphological table can be constructed by identifying and comparing multiple design options for each function. Furthermore, material selection is addressed separately, as no single material can meet the diverse mechanical demands of all components. A dedicated comparison table 5 presents a detailed overview of candidate materials, including their densities, advantages, and limitations.

Materials Among metallic materials, aluminum and steel stand out as the most relevant options. Steel is reserved for components subject to high mechanical loads and structural constraints, where rigidity and strength are critical. Aluminum, by contrast, is the preferred choice due to its low cost, light weight, and excellent machinability. Titanium is not considered suitable for this application, as the

Table 5: Comparison of Structural Materials for Robotics

Material	**Density (g/cm^3)**	**Pros**	**Cons**
Carbon Fiber	1.75	Very high strength-to-weight ratio, corrosion-resistant, durable, good design flexibility. Very rigid, excellent corrosion resistance	Expensive, brittle, not ideal for high structural loads, difficult to repair. Not ideal for heavy loads, high cost, brittle
Aluminum	2.70	Lightweight, corrosion-resistant, cheap, easy to shape and repair. Easy to machine and shape, relatively strong	Heavier than carbon fiber, prone to dents/scratches, not suitable for extreme loads. Less rigid than carbon fiber, corrosion in extreme conditions
Glass Fiber	2.50	High thermal resistance, improved rigidity and strength, flame retardant, good impact resistance. Improves plastic rigidity, good shock resistance	Opaque, more brittle, poor fluidity, high injection temps/pressure, absorbs water. Makes plastics more brittle, absorbs humidity
Kevlar (Aramid)	1.43	Very light, excellent abrasion and fatigue resistance, good thermal resistance, high strength-to-weight. High impact and abrasion resistance	UV-sensitive, poor adhesion to epoxy, water absorption, expensive. UV degradation, weak resin adhesion
Steel	7.85	Very strong, high wear resistance, good for industrial applications	Heavy, may require coatings, not ideal for mobile robots
Titanium	4.5	High strength-to-weight, corrosion-resistant, biocompatible, ideal for aerospace/medical	Very expensive, hard to machine, not widely accessible
Plastics (e.g., ABS, Nylon)	1.10 (abs) 1.24(pla) 1.14(nylon)	Lightweight, low-cost, versatile, good electrical insulation	Lower strength and heat resistance, not for heavy-duty use
Ceramics	2.5-6	High heat and wear resistance, good electrical insulation, very hard	Brittle, expensive, hard to machine
Smart Materials	—	Adaptive properties, suitable for biomimetic/medical use, energy harvesting	High cost, complex integration, hard to mass-produce

mechanical requirements do not justify its exceptional performance, and its high cost—as well as the complexity of its manufacturing—make it impractical.

Regarding composite materials, carbon fiber and glass fiber appear to be promising candidates for lightweight components with complex geometries that are subjected to significant mechanical stresses. Fiber-reinforced plastics—such as carbon fiber-reinforced polymers—may offer a good compromise between mechanical performance and cost, especially when low weight and moderate strength are required.

Other materials are not deemed relevant within the scope of this project. Ceramics and smart materials are either too complex to manufacture, too fragile, or prohibitively expensive. Moreover, some of their key advantages, such as high thermal resistance or adaptive properties, are not applicable or necessary in this context. Therefore, their integration would add unnecessary complexity without providing functional benefit.

Motorization Choice For the motorization system, three possible type of motorisation: electric, pneumatic and hydraulics. The electric motors have been selected. This choice is motivated by several key factors. Electric motors operate quietly compared to pneumatic and hydraulic systems, which require pumps and compressors that generate significant noise. These components also require additional infrastructure such as tanks, making the system more complex and less practical. The robot is intended to be used in an office environment, where such equipment is not available and would hinder mobility—for example, when moving the device from one room to another. In addition, electric motors offer a fast response time and are easier to maintain than the other technologies. As a result, all the concept variants presented in this work are based exclusively on electric motors. No comparative evaluation of the three motorization technologies is included, as electric motors are clearly the most appropriate solution for the intended application.

Explanation	Figures				
Active translation transmission	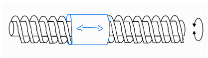 Figure 12: Screw transmission	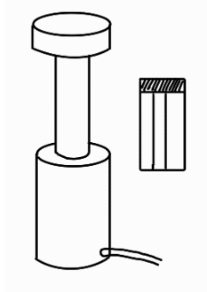 Figure 13: Piston	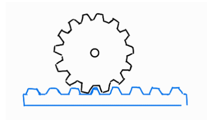 Figure 14: Rack and pinion	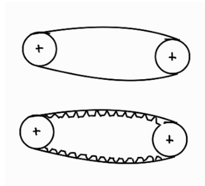 Figure 15: Belt and toothed belt	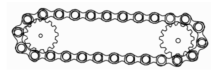 Figure 16: Chain transmission
Maintaining the robot's position on the tabletop	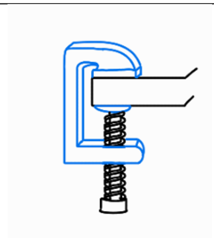 Figure 17: Clamp	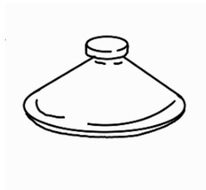 Figure 18: Suction cup	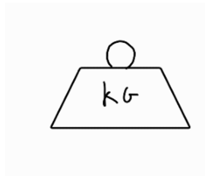 Figure 19: Structure weight	 Figure 20: Attached to the table	
Structure layout	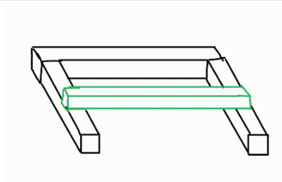 Figure 21: U structure				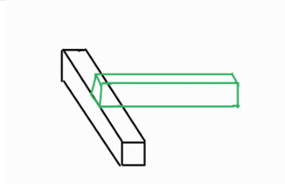 Figure 22: T structure

Table 6: Morphological table 1

Explanation	Figures
Adjustable pen orientation	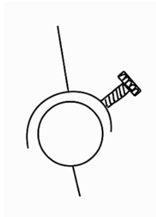 Figure 23: Lockable ball head 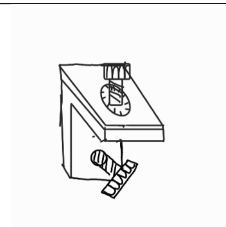 Figure 24: Lockable two direction independent rotation mechanism
Pen holder	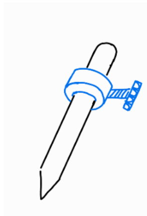 Figure 25: Ring with pressure screw 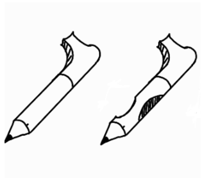 Figure 26: Custom pen with or without finger pad 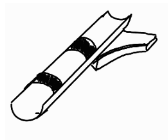 Figure 27: Pen with support clamp  Figure 28: Chuck-like mechanism 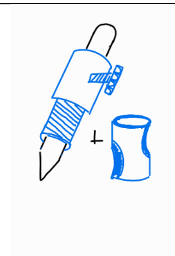 Figure 29: Hollow tube with pressure screw and screw-able finger pad 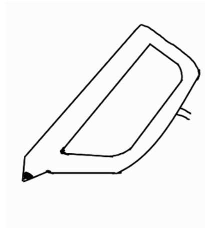 Figure 30: Custom two contact point pen design  Figure 31: Clamp
Passive Z-axis translation	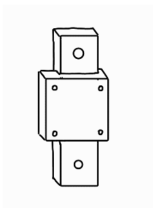 Figure 32: Linear guide 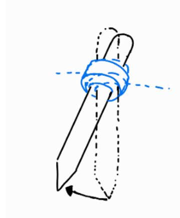 Figure 33: Rotation of the pen

Table 7: Morphological table 2

4.4 Concept variant

Base on the morphological tables 6 7, six concept variant were established. each of them are presented down below with a description to help the good understanding of the variant.A colour code was used in the drawing to ease the reading-ness: red for motorization, purple for the active translation mechanism, yellow for the transmission, blue for the pen orientation, orange for the pen design, green for the second arm the one responsible for the second axis translation.

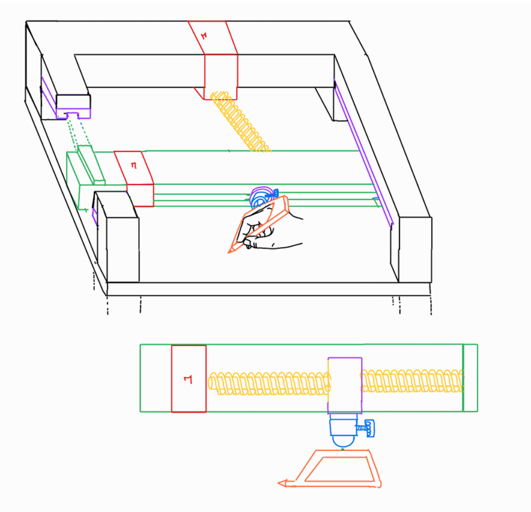

(a) Concept 1

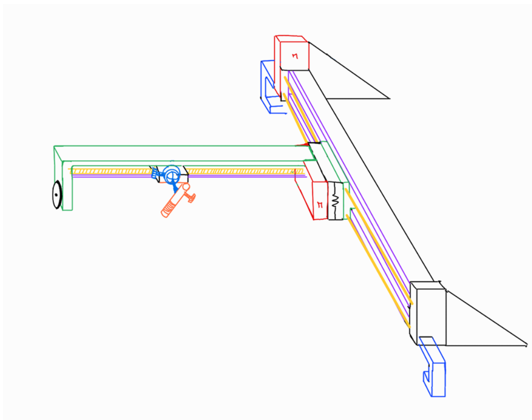

(b) Concept 4

Figure 34

Concept variant 1(Figure 34a): This first variant adopt a "U" shaped structure and employs a screw transmission system (highlighted in yellow), where the rotating screw drives a moving nut attached to the carriage. As the carriage travels along the axis, it extends towards the rear of the device, thereby requiring additional space at the back for safe enclosure and protection of both the screw mechanism and the user. The structural layout forms an inverted U-shape surrounding the writing area. This configuration includes vertical side elements that may interfere with the natural arm positioning of the user—regardless of whether they are left- or right-handed—potentially leading to discomfort or obstruction during writing tasks. The translational motion is guided by linear rails (shown in purple and green), ensuring precise movement of the mechanism. Vertical movement (Z-axis) is not implemented as a true translation but as a rotation around a fixed axis at the pen holder. This rotation raises the pen tip off the paper and is considered suitable, given that the typical lifting height required during handwriting is approximately 1-2 cm, which can be achieved by this motion. Pen orientation is handled using a ball joint mechanism, secured in place with a locking system. The writing instrument used in this variant is a custom one-piece pen with a trapezoidal shape. This geometry is intended to distribute the applied forces across two distinct contact points, promoting ergonomic handling. Finally, the entire device is fixed directly to the tabletop without any integrated repositioning system, resulting in a stable but non-movable setup during operation.

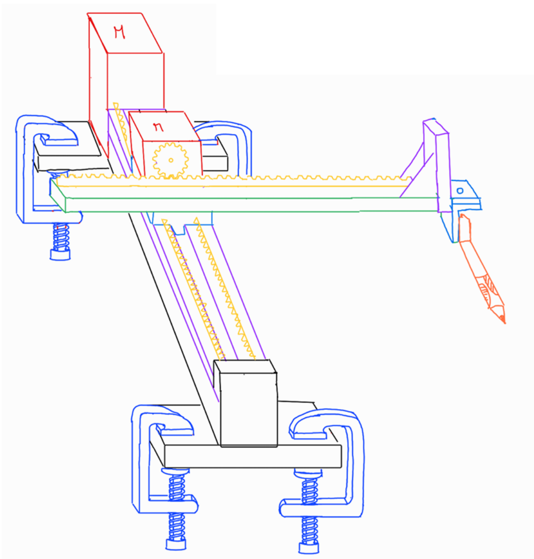

(a) Concept 2

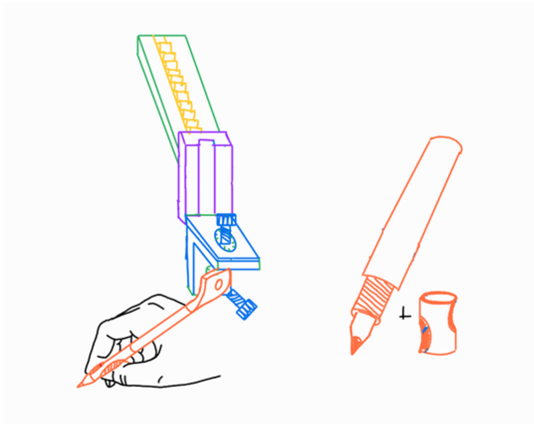

(b) Concept 2 pen orientation and Z-axis translation

Figure 35

Concept variant 2(Figure 35a): This variant has a smaller structure, with only one guide per translation. The transmission systems consist of belts and a rack-and-pinion mechanism. These would obviously be hidden under protective covers, but for clarity in the drawings, the protections were not shown. The translation is guided by a single linear guide for each axis. The Z-axis movement is achieved with a vertical slider that allows free up-and-down motion of the whole green arm, the weight is counterbalanced by a constant force spring. Pen orientation is adjusted using a mechanism that decouples the two possible rotational axes, allowing independent adjustment. The mechanism is locked in place using pressure screws. The pen is held from the top and is custom-made. Its upper part is designed to be fixed to the orientation mechanism. The pen also includes finger positioning features to help guide the user in holding it correctly. Several finger positioning layouts can be used, as they are attached to the pen by screwing them. The device is fixed to the table using clamps, which allows for easy repositioning and manual adjustment of the device on the working surface.

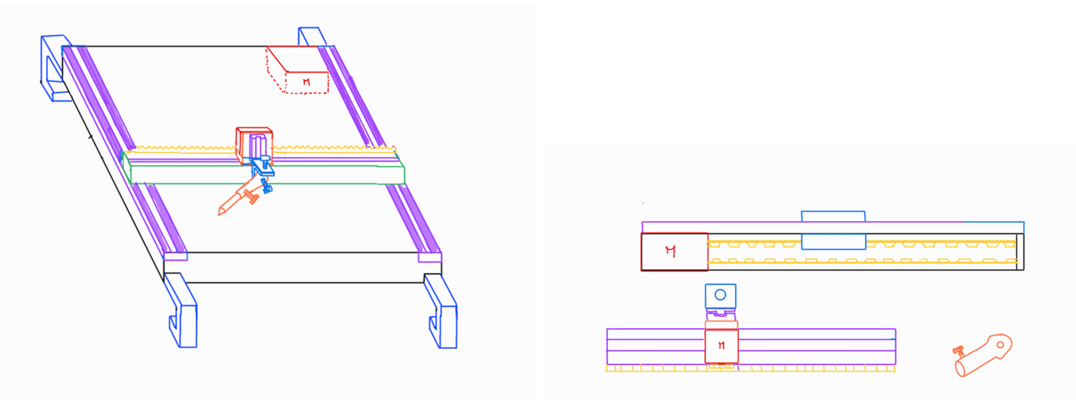

(a) Concept 3

(b) Concept 3 open view of transmission

Figure 36

Concept variant 3(Figure 36a): This variant addresses the issue encountered in the first concept, where the structure interfered with the user's arm. Here, the first axis translation occurs at the same level as the writing surface. The structure includes a second surface—referred to as the writing level—positioned above the table. The translation guides are placed at this writing level, meaning they do not obstruct the user's arm during use. The transmission systems used are rack-and-pinion and belt mechanisms. The translation is guided by two linear guides positioned at writing level. The Z-axis translation is achieved with a vertical slider, allowing free vertical movement. Pen orientation is managed with the same mechanism as in variant 2, enabling independent adjustment of two rotation axes and locked in place using pressure screws. The pen is fixed using a hollow tube and a pressure screw. This setup allows the user to insert and use their preferred pen model. The entire device is secured to the table using large clamps that pass through the structure and beneath the writing level. These clamps are adjustable in width and are tightened using pressure screws.

Concept variant 4(Figure 34b): This variant uses the same clamping system as the third one. The structure adopts a "T" configuration, with each translation using a single linear guide as defined in the morphological table. The transmission systems consist of a combination of lead screw and belt. For the screw, the screw rotates while the attached carriage moves linearly. The guidance is provided by linear guides for both translations. Additionally, the second arm (in green) is supported at its far end by a wheel to enhance stability. The Z-axis motion is achieved by moving the entire arm vertically along a sliding rail. Since the whole arm moves with the user's input, its weight is compensated by a constant force spring. Pen orientation is achieved using the same mechanism as in the first concept, based on a ballhead and locking system. The pen is held in a hollow tube with a pressure screw and features an interchangeable tip, similar to the one used in variant 2. The entire system is clamped to the table using the same adjustable manual clamping system as in concept 3.

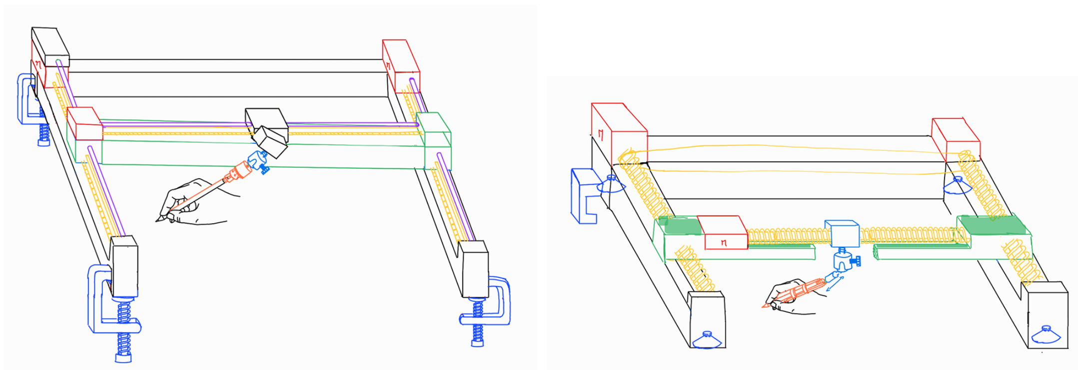

(a) Concept 5

(b) Concept 6

Figure 37

Concept variant 5(Figure 37a): This variant features a "U"-shaped structure and includes three motors: two for the first translation axis -that needs to be synchronized- and one for the second. The transmission is entirely achieved using belts, and both axes are guided by linear rails. However, the structure presents the same drawback as variant 1, where the positioning of the structure may cause discomfort for the user's arm. The Z-axis motion is achieved through the rotation of the entire chain composed of the pen, pen holder, and lockable ballhead. Pen orientation is managed using a ballhead mechanism that allows angular adjustment. The pen is freely chosen by the user and is fixed from the top using a chuck-like mechanism. The device is mounted directly on the table.

Concept variant 6 (Figure 37b): This final variant also features a "U"-shaped structure and includes two motors, but three transmission systems: two for the first translation axis and one for the second. The first axis uses two synchronized transmission systems to ensure good guidance. The synchronization between the two sides is achieved with a belt. The second axis is also driven by a belt transmission. All translations are guided using linear rails. The green arm is shown in two parts for clarity in the drawing, but it is actually a single piece. The Z-axis motion is not aligned with the global Z-axis but instead follows the axis of the pen. The pen is lifted by sliding it alongside its lengthwise direction, which creates the required tip elevation. Pen orientation is controlled using a ballhead mechanism, consistent with earlier variants. The pen is placed in a semi-open holder with two clamps near its ends to keep it in position during use. The pen itself can be freely chosen by the user. The device is held in place on the table using a combination of suction cups and clamps

4.5 Evaluation

The evaluation of the different concept variants is based on a set of weighted criteria, which are categorized according to the design aspects they assess. These categories are: transmission performance, structural design, and pen integration. The evaluation remains qualitative and comparative in nature, as no precise numerical measurements are applied at this stage.

The weight of each criterion ranges from 1 to 3, with 1 representing a minor criterion and 3 indicating a major or highly influential one. The six concept variants are evaluated using these criteria. The scores assigned in the table take values between -1 and 1 . A score of 1 indicates that the concept meets the criterion effectively. A score of 0 is assigned when the performance is neutral or average. A score of -1 denotes that the concept performs poorly on the criterion compared to the other variants.

The first category focuses on transmission performance and includes the following four criteria:

- **Movement fluidity**: Rack and pinion mechanisms are generally less smooth than belt or screw systems due to the discrete engagement of teeth, which can introduce small interruptions in motion.

  Score: belt = 1 ; screw = 1 ; rack and pinion = -1

- **Transmission robustness**: Belts tend to wear more quickly than rack and pinion or screw mechanisms, particularly when made of rubber. Rack and pinion systems exhibit more wear than screws due to repeated contact between the gear teeth.

  Score: belt = -1 ; screw = 1 ; rack and pinion = 0

- **Noise level**: Rack and pinion systems typically produce more noise compared to belts or screws.

Score: belt = 1 ; screw = 1 ; rack and pinion = -1

- **Ease of maintenance**: Belts can be replaced with minimal disassembly, whereas repairing or replacing rack and pinion or screw systems generally requires more extensive disassembly of the device.

  Score: belt = 1 ; screw = -1 ; rack and pinion = 0

The second category assesses structural design through five criteria:

- **Device footprint**: This refers to the total space occupied by the system. Although not measured quantitatively, a qualitative comparison is used. Some concepts require workspace on both sides of the first translation axis, effectively doubling the required area (e.g., variants X and X).
- **Ease of installation**: The fixation system should allow for quick and straightforward installation, ideally without tools, and should be operable by non-specialist users.
- **Motion guidance quality**: As high precision is required, the structure must effectively support the loads generated by the moving arm (identified in green in the schematics).
- **Writing visibility**: The user should have a clear and unobstructed view of the writing area, as visual feedback is essential for accurate handwriting.
- **Arm comfort**: The user should not experience discomfort while writing and should be able to maintain a natural and relaxed arm posture throughout the interaction.

The third category concerns pen design and includes three criteria:

- **Ergonomics**: The pen design should provide a comfortable grip and accommodate a variety of hand sizes and grasping styles, minimizing user discomfort.
- **Force distribution**: The writing forces transmitted through the pen should be evenly distributed to avoid stress concentrations and prevent the pen from breaking.
- **Vertical motion quality**: The vertical translation of the pen should closely replicate natural pen-lifting gestures used in handwriting.

Since the three groups of criteria—Transmission, Structure, and Pen—are considered orthogonal, meaning they address independent aspects of the design, the subtotal for each group is presented separately. This allows for identifying the most suitable solution within each specific design dimension.

In Table 8, in some transmission-related criteria, intermediate scores such as 0.5 or -0.5 appear. These reflect the presence of multiple transmission types within a single variant. Each type is individually scored on the same scale, and an average is computed to represent the overall transmission performance of the robot.

Group	Criteria	Weight	1	2	3	4	5	6
Transmission	Movement fluidity	3	1	0.5	0.5	1	1	1
Transmission	Transmission robustness	2	1	0	-0.5	0	-1	1
Transmission	Noise level	1	1	0	0	1	1	1
Transmission	Ease of maintenance	1	-1	0.5	0.5	0	1	-1
Transmission Subtotal			**5.0**	**2.0**	**1.0**	**4.0**	**3.0**	**5.0**
Structure	Device footprint	2	-1	-1	0	0	0	0
Structure	Ease of installation	1	-1	0	1	1	1	1
Structure	Arm comfort	2	-1	1	1	-1	-1	-1
Structure	Motion guidance	3	1	-1	1	-1	1	1
Structure	Writing visibility	1	1	1	1	-1	1	0
Structure Subtotal			**-1**	**-2**	**7**	**-5**	**3**	**2**
Pen	Vertical motion quality	1	-1	1	1	-1	-1	0
Pen	Ergonomics	2	1	1	0	0	0	-1
Pen	Force distribution	3	1	0	-1	0	-1	-1
Pen Subtotal			**4**	**3**	**-2**	**-1**	**-4**	**-5**
Total		**22**	**8.000**	**3.000**	**6.000**	**-2.000**	**2.000**	**2.000**

Table 8: Evaluation table grouped by design aspects: Transmission, Structure, and Pen integration

Final Concept Selection An analysis of the evaluation scores indicates that Concept 1 achieves the highest overall rating, closely followed by Concept 3. At the subgroup level, both concepts exhibit superior performance in different design categories. According to design methodology, such situations call for an iterative approach in which the most relevant features from the best-performing concepts are combined into a new, optimized solution.

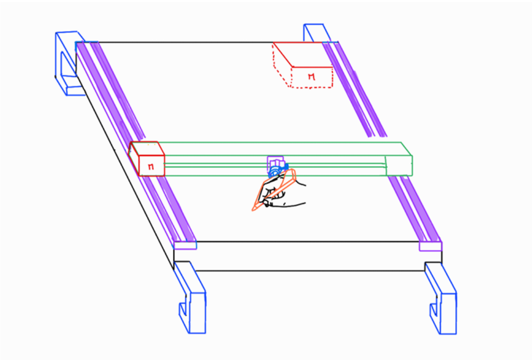

(a) Final concept

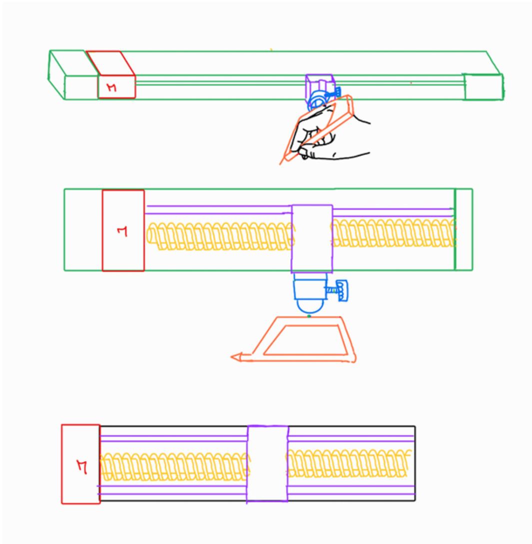

(b) Final concept transmission

The resulting concept integrates:

- a screw transmission system, as implemented in Concept 1;
- the structural layout of Concept 3, which offers a significant advantage by eliminating constraints on the user's arm positioning;
- a custom-designed pen with two contact points, aimed at improving ergonomic support and force distribution.

To ensure that this revised design outperforms the previous variants, it has been re-evaluated using the same criteria. The results, presented in Table 9, confirm unambiguously that this solution surpasses all others.

This final design is illustrated in Figure 38a, using the same color coding as in the previous concept representations.

Group	Criteria	Weight	Final Score	Weighted Score
Transmission	Movement fluidity	3	1	3
	Transmission robustness	2	1	2
	Noise level	1	1	1
	Ease of maintenance	1	-1	-1
Transmission Subtotal				**5**
Structure	Device footprint	2	0	0
	Ease of installation	1	1	1
	Arm comfort	2	1	2
	Motion guidance	3	1	3
	Writing visibility	1	1	1
Structure Subtotal				**7**
Pen	Vertical motion quality	1	-1	-1
	Ergonomics	2	1	2
	Force distribution	3	1	3
Pen Subtotal				**4**
Total		**22**		**16**

Table 9: Final evaluation of the selected concept, grouped by design category.

5 Prototype

With the design now established, a first prototype can be assembled to evaluate the performance and relevance of the choices made so far. For this prototype, the use of off-the-shelf components from commercial suppliers is preferred. The idea is to build it in a modular way, similar to a Lego set, using readily available parts. The budget for the project is 3000 euros. The linear guides are from **Igus**, a company specialized in modular, low-friction linear solutions. The motors are from **Maxon**, a manufacturer renowned for its reliable and high-performance electric motors, particularly in robotics applications. The mechanical components are sourced from **Misumi**, a major supplier known for its customizable parts and fast delivery. The only exceptions are the ball head and a distance sensor, which are sourced from **Neewer** and **RS-Online**, respectively. All other custom parts will be manufactured at **CREDEM**. This section presents the different components grouped into their respective sub-assemblies, followed by their integration into the global prototype. A summary of the prices, references, and suppliers of the purchased components is provided at the end of the section. For each in-house manufactured component, the material and proposed manufacturing process are also indicated.

5.1 Y translation

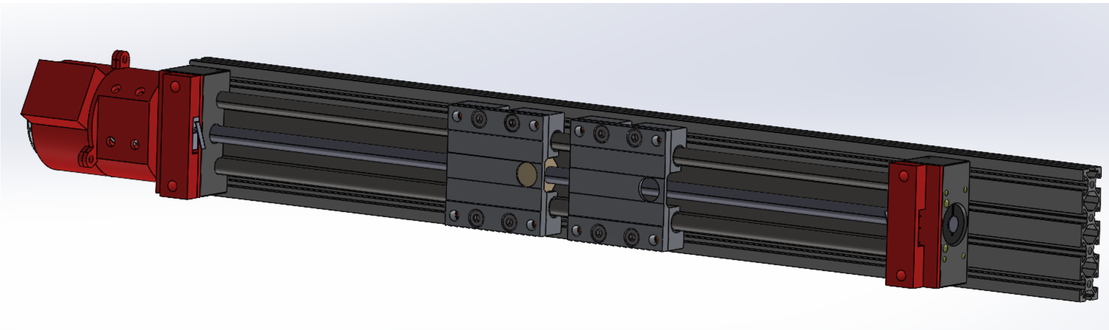

Figure 39: Y translation assembly

Leadscrew For the leadscrew transmission, the SLW-1040 model from Igus was selected. The choice was made using the configurator available on the Igus website, based on key input parameters such as the required speed, acceleration, travel length, and load. The configurator provided a set of suitable solutions. Among these, the pitch and the price were the main selection criteria. The smallest available pitch was 12 mm, followed by 20 mm. Given the required positioning accuracy of

0.15 mm, the 12 mm pitch was preferred. Price considerations then guided the final selection among the remaining models. For this axis, two carriages are mounted on the linear guide: one is actuated by the screw, while the other remains passive. The use of two carriages allows the system to better withstand lateral forces and provides improved support in the X and Y directions. This configuration increases the overall stiffness of the system and contributes to higher stability and accuracy during operation.

Motor To perform the motor sizing for this application, the motor sizing tool provided by Oriental Motor [35] was used. The input parameters are summarized in Table 10

The tool returned a required torque of 0.56 N m. The required motor speed is derived from the lead screw's linear speed and lead: with a target speed of 0.12 m/s and a lead of 12 mm, the resulting minimum rotational speed is 600 rpm, this the speed so that the robot can reach its maximum linear speed, any motor with lower rotational speed than 600 rpm is not possible.

Parameter	Value	Justification
Linear speed	120 mm/s	Defined in specification requirements
Lead	12 mm	Selected for required resolution and force
Length	350 mm	Maximum required stroke for movement
Friction coefficient of the guide	0.2	Estimated from Igus material pairing (steel/iglidur) [36]
Mass to move	3.6 kg	Estimated from CAD and component weights
Screw diameter	10 mm	Set by selected Igus SLW-1040 screw
Screw efficiency	67%	Manufacturer data from Igus [37][2]
External force	110 N	Maximum force expected during operation
Accuracy	0.15 mm	Required to match human handwriting resolution
Safety factor	1.5	Safety margin to ensure reliability

Table 10: Motor sizing parameters and their justification

According to the Maxon catalog, the most suitable motor is the EC 60 Flat, 200 W, 48 V. Its nominal torque is 0.58 N m and its nominal speed is 3000 rpm, which exceeds both required values. The complete datasheet is provided in Appendix 2.

[2] Igus provides the following formula to determine lead screw efficiency [37]:

$$\eta = \frac{\tan\alpha}{\tan\big(\alpha + \tan^{-1}(\mu)\big)}, \quad \alpha = \tan^{-1}\left(\frac{\text{lead}}{\pi \cdot \text{diameter}}\right), \quad \mu = 0.15$$

This value is given for iglidur® J under dry operating conditions.

A MILE encoder with 4096 counts per turn is integrated to enable precise rotor position measurement. The motor is controlled using the ESCON2 Micro 60/5, a four-quadrant servo controller for DC and EC motors.

One potential drawback of this motor is the presence of torque ripple, resulting from a combination of cogging torque and commutation ripple. Cogging torque is due to the variation in magnetic reluctance as the rotor moves between magnetic poles, whereas ripple torque is associated with block commutation. These effects can lead to irregularities in the motion of the end-effector, which is particularly undesirable in handwriting applications.

The ripple torque can be mitigated using sinusoidal commutation, also known as Field-Oriented Control (FOC), which is supported by the ESCON2 controller. Cogging torque, on the other hand, cannot be completely eliminated. Custom control strategies exist to minimize it, but they are typically complex and costly. According to Maxon documentation [38], cogging torque is mainly perceptible at very low speeds (below 10 rpm). In this application, the motor typically operates at around 100 rpm, so cogging effects are expected to be negligible.

A second potential issue with this motor is overheating during low-speed, high-torque operation. At low speeds, the self-cooling effect generated by rotor ventilation is insufficient, which may lead to a rapid rise in motor temperature. To address this, the addition of an external cooling fan may be considered, in further work, to ensure thermal stability during prolonged use.

Structure The linear guide is fixed on a 20x80x650 aluminium profile (ref: HFSP5-2080-650) from Misumi. On each side of the linear guide two end of range switch (ref: SS-5GLT) are placed(see Figure 39. Those switch are placed for the calibration of the robot to know at which position of it rotor correspond each end of the guide. to protect it all a thin metal sheet is placed on top of the guide to avoid people to hurt themselves with the transmission.

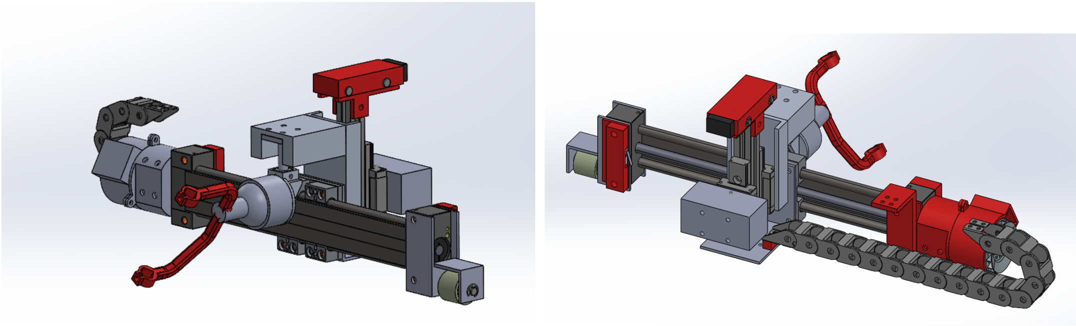

(a) Front view (b) Rear view

Figure 40: X translation assembly

5.2 X translation

The linear guide used for the X-axis is identical to the one employed for the Y-axis, except for its length, which is 240 mm. Mounted on the carriage are the components responsible for the Z-axis translation, the force sensor, and the pen orientation mechanism. This guide is connected at one end to the Y-axis guide through an assembly of metal piece. At the opposite end, a free-rolling wheel (ref: RORUAP30-20 and hinge pin ref: HCCG8) mounted on a bearing is attached to support the vertical load generated by the Z-axis assembly, without adding resistance to the X translation. A cable carrier (ref: MHPKS202-30-15-A) is also mounted on the carriage to organize and secure the wiring[3]. Additionally, two contact switches(ref: SS-5GLT) are placed at each end of the guide to serve as limit switches for calibration and safety purposes.All of these elements are shown in Figure 40.

[3] In Figure 46, the cable carrier appears unattached at one end. This is due to limitations in the CAD model, which does not allow manual positioning of the cable carrier. As a result, in order to display the correct number of links, the carrier could not be attached to its support.

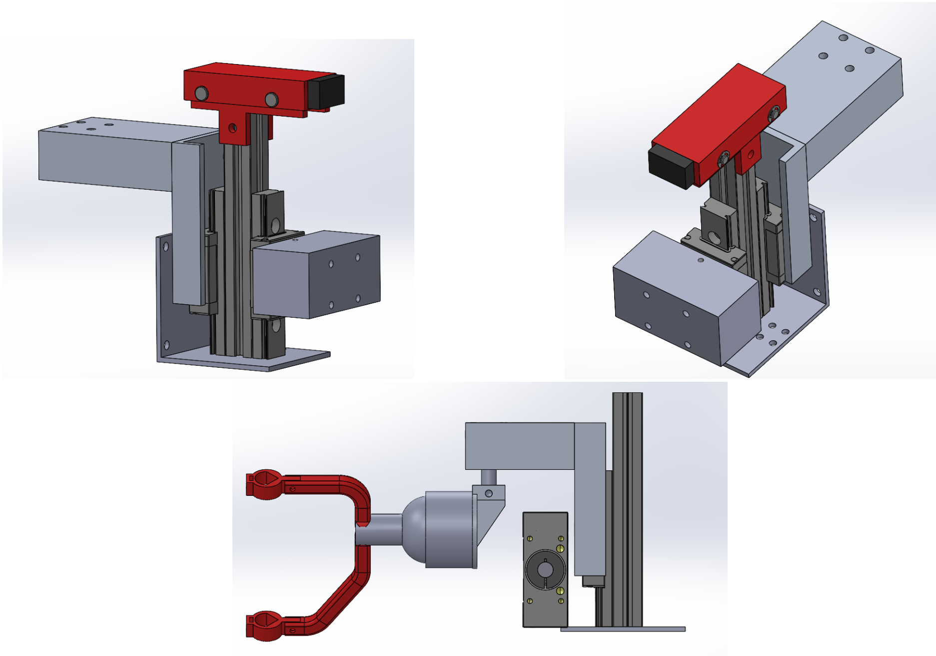

Figure 41: Different view of the Z-axis translation mechanism

Z-axis translation The Z-axis is guided by two miniature profiled rail guides mounted (ref:SSEBZ20) on an aluminum profile (ref: HFSP5-2020-150). A pulley mechanism is installed at the top of this structure. On one of the guides, the sensor and pen orientation assembly is mounted, while on the opposite guide, a counterweight with equal mass is attached and the both are link with a cable passing through two pulley(ref: SZU6-16 and hinge pin ref: HCCG6-36), as shown in Figure 41. This configuration ensures weight compensation, so the user does not need to exert significant force to lift the pen, thus preserving writing fluidity and avoiding motion disruption. A distance sensor (ref: OPB720B-06Z) is fixed onto the pulley housing using adhesive (see Figure 41. This sensor is used to detect the vertical position of the pen. During an initial calibration phase, the distance between the sensor and the counterweight is recorded when the pen is in contact with the surface. Later, during operation, this distance is continuously monitored and compared to the reference value to determine whether the pen is lifted or not.

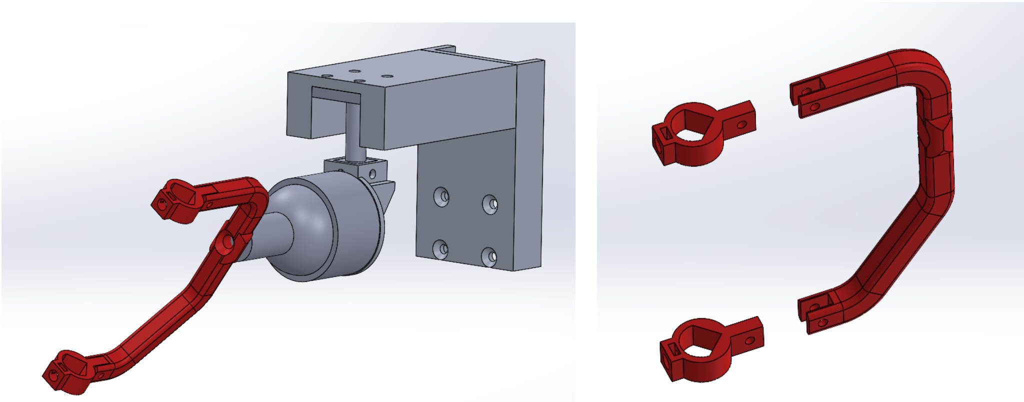

(a) Pen holder assembly

(b) Pen support

Figure 42: Pen Holder and orientation

Pen Holder and orientation As shown in Figure 42,the pen holder and sensor assembly is mounted on a custom L-shaped support made of two aluminum parts, fixed to the miniature profiled rail guides(ref: SSEBZ20) of the Z-axis. This L-shaped design is intended to orient the lead screw and carriage away from the user, thereby improving user safety by minimizing exposure to moving components. A custom-made bi-axial force sensor is mounted on this support, capable of measuring forces up to 110 N in both the F_x and F_y directions. A mounting interface for the ball head is fixed directly onto the sensor, with the ball head itself oriented to face the user, enabling intuitive manipulation of the pen. The ball head is the NEEWER GM36 36mm Metal Panorama Low Profile Camera Tripod Ball Head. The pen holder is composed of three parts rather than a single integrated piece. This design choice was made because the prototype stage requires easy adjustment and simpler fabrication. The pen is held by two ring-shaped elements with pressure screws. These rings are attached to a C-shaped support that features a central hole for attachment to the ball head. The inner surfaces of the rings include a V-groove profile, ensuring the correct alignment of the pen by maintaining two consistent contact points.

5.3 Structural Analysis

Two assemblies were analysed to make sure they behave correctly under the forces applied during use. The simulations were done with SolidWorks Static Simulation, and all parts are made from 2024-T3 aluminum alloy. The goal was to check that the deformations stay below the robot's required precision of 0.15 mm, so they don't affect the user's handwriting.

The first part connects the Y-axis to the X-axis translation (see Figure 43). It needs to remain rigid, because if it bends, the X-axis carriage could lose its perpendicularity with the Y-axis, which would reduce motion accuracy. The simulation was performed with a force of 110 N applied in the Y direction.

The second part is an L-shaped piece that links the sensor and pen holder to the profiled rail guide (see Figure 42). If it bends, the pen holder may shift sideways, which would reduce writing precision. Simulations were performed with a 110 N force applied in both the X and Y directions.

In both cases, the simulations confirmed good mechanical behavior, with deformations remaining below 0.15 mm – the required precision of the robot – validating the design and dimensions of the parts.

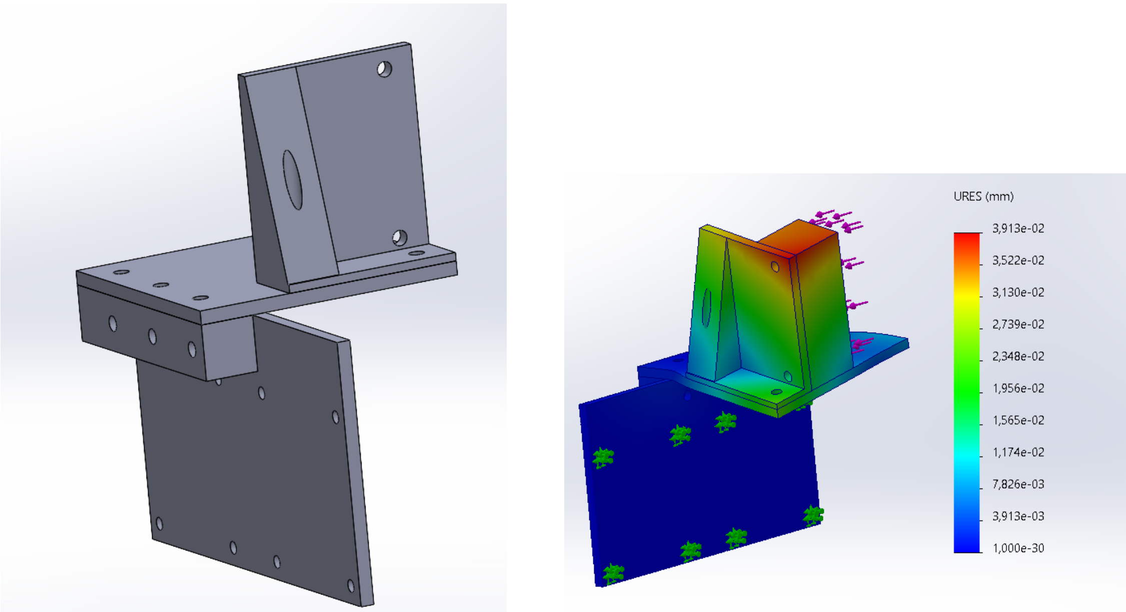

Figure 43: Simulation result with a 110 N force on the first part

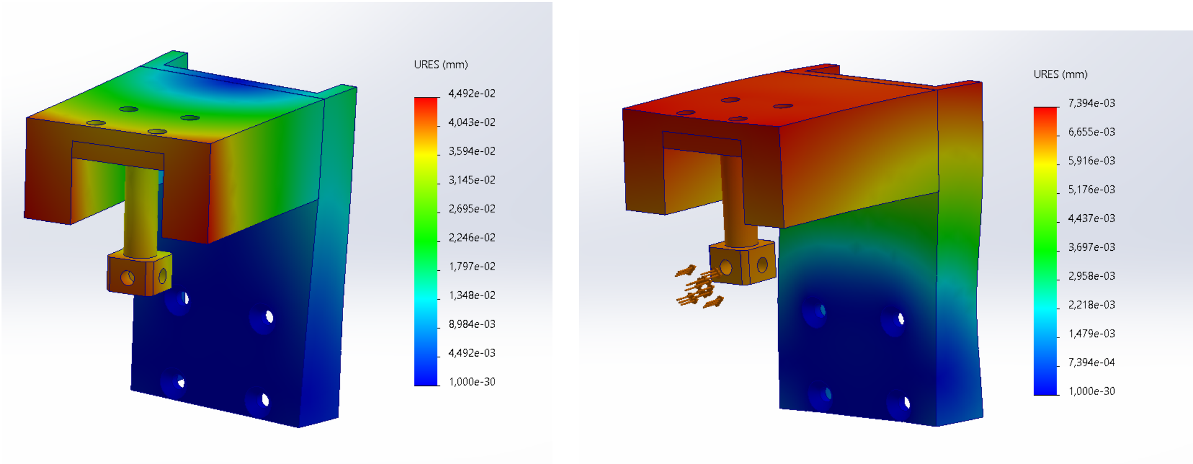

(a) Force of 110 N in the Y direction

(b) Force of 110 N in the X direction

Figure 44: Simulation results for the L-shaped part

5.4 Global prototype

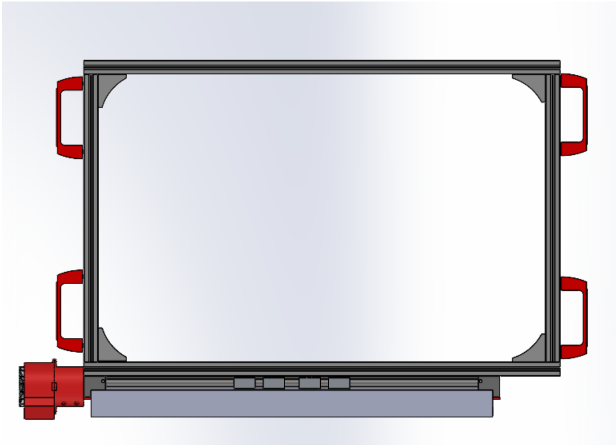

Figure 45: Prototype structure

The remaining structure consists of a second $20 \times 80 \times 650$ mm aluminum profile (ref: HFSP5-2080-600) running parallel to the Y-axis rail, and two perpendicular $20 \times 20 \times 392$ mm profiles(ref: HFS5-2020-392) connected with brackets to form a stable rectangle frame(see Figure 45). A wooden board of dimensions $450 \times 650 \times 12$ mm serves as the tabletop(see Figure 46). Holes are drilled and counterbored so that the screw heads are recessed below the surface. The recesses are then filled with mastic to create a flat working surface without any protrusions that could interfere with writing or hand movement. Finally, two handles (ref: UPCN21-R-36) are attached to the front and back aluminum profiles(see Figure 45) to facilitate transport and to provide a safe grip point for lifting the prototype without damaging any components. The Solidworks assembly, all the parts and datasheets are available in the appendix submitted with the thesis.

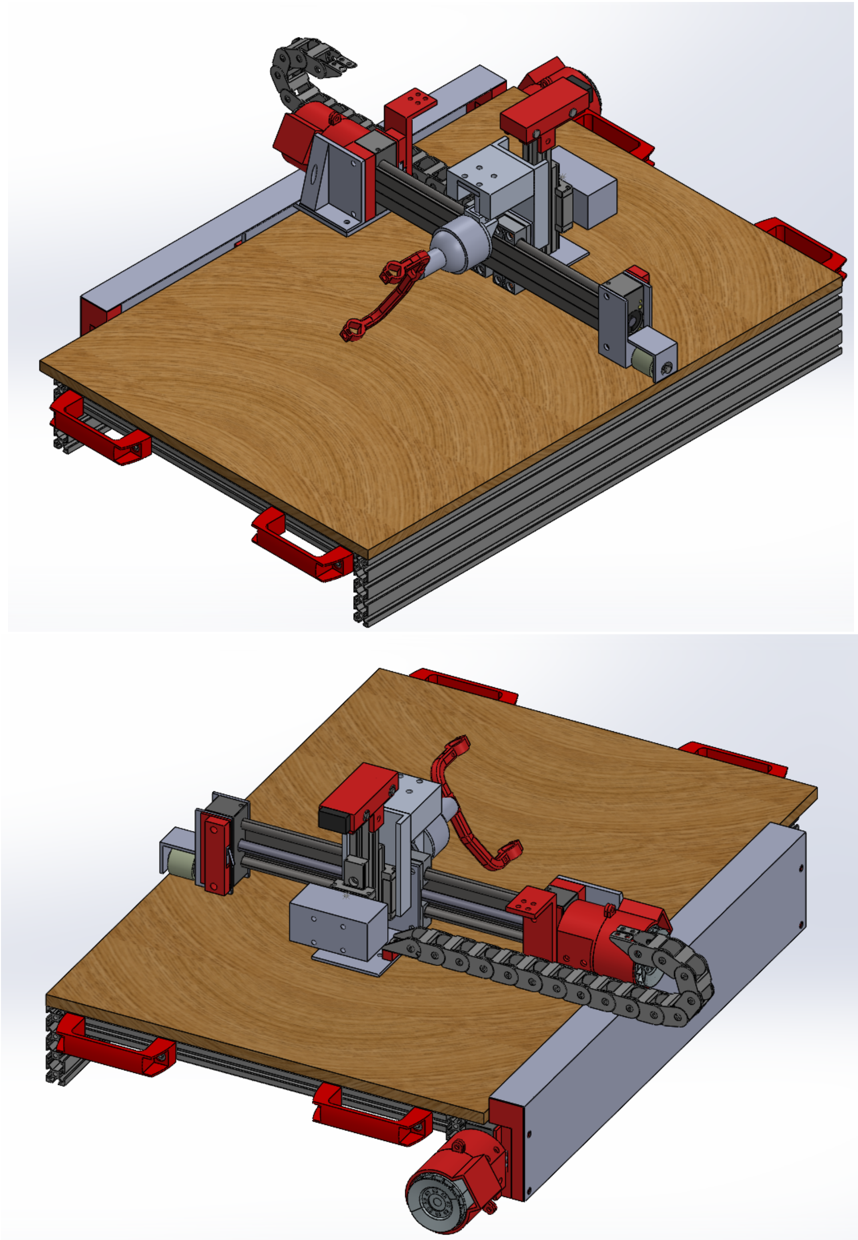

Figure 46: Global prototype views

5.5 Pricing and reference

The following Table11 lists all dealer-supplied components and their corresponding prices.

Component	Website	Price	Quantity	Total price
Module linéaire drylin® : SLW-1040 DS10x12	https://www.igus.be/product/20275?C=BE&L=fr&artNr=DL-SLW-0549	211,56	1	211,56
Module linéaire drylin® : SLW-1040 DS10x12	https://www.igus.be/product/20275?C=BE&L=fr&artNr=DL-SLW-0549	258,63	1	258,63
NEEWER Rotule 36mm Panoramique Low Profile en Métal	https://fr.neewer.com/products/neewer-low-profile-camera-tripod-ball-head-66600998	49,99	1	49,99
EC 60 flat Ø60 mm, sans balais, 200 W, avec capteurs à effet Hall Codeur MILE 4096 impulsions, 2 canaux ESCON2 Micro 60/5, servo-contrôleur	https://www.maxongroup.fr/maxon/view/catalog/?target=combination0 https://www.maxongroup.fr/maxon/view/catalog/?target=combination0 https://www.maxongroup.fr/maxon/view/catalog/?target=combination0	569,99	2	1139,98
RORUAP30-20	https://fr.misumi-ec.com/vona2/detail/110300422220/?HissuCode=RORUAP30-20	22,13	1	22,13
HCCG8	https://fr.misumi-ec.com/vona2/detail/110300095750/?HissuCode=HCCG8	12,21	1	12,21
UPCN21-R-36	https://fr.misumi-ec.com/vona2/detail/110302239150/?PNSearch=UPCN21-R-36	6,66	4	26,64
SSEBZ20	https://fr.misumi-ec.com/vona2/detail/110302586530/?HissuCode=SSEBZ20	64,07	2	128,14
HBLFSSW5	https://fr.misumi-ec.com/vona2/detail/110300437350/?HissuCode=HBLFSSW5	2,39	4	9,56
HFS5-2020-392	https://fr.misumi-ec.com/vona2/detail/110302683830/?HissuCode=HFS5-2020-392	2,49	2	4,98
HFSP5-2080-650	https://fr.misumi-ec.com/vona2/detail/110302685930	69.43	2	138.86
HFSP5-2020-150	https://fr.misumi-ec.com/vona2/detail/110302685660/?HissuCode=HFSP5-2020-150	18.00	1	18.00
HCCG6-36	https://fr.misumi-ec.com/vona2/detail/110300095750/?HissuCode=HCCG6-36	11,49	2	22,98
SZU6-16	https://fr.misumi-ec.com/vona2/detail/110302274060/?HissuCode=SZU6-16	10,96	2	21,92
HNTTV5-5	https://fr.misumi-ec.com/vona2/detail/110302607960	0,56	30	16,8
MHPKS202-30-15-A	https://fr.misumi-ec.com/vona2/detail/110302549860	31,35	1	31,35
OPB720B-06Z Optek	https://befr.rs-online.com/web/p/reflective-optical-sensors/0414197	19,2	1	19,2
SS-5GLT	https://fr.misumi-ec.com/vona2/detail/221000559138/?HissuCode=SS-5GLT&PNSearch=SS-5GLT&KWSearch=ss-5glt&searchFlow=results2products&list=PageSearchResult	2.16	4	8.64

Component	**Website**	**Price**	**Quantity**	**Total price**
COU-AR-K-080-100-25-26-B-AAAA	https://www.igus.fr/product/drylin_E_coupling_toothed_belt?artnr=COU-AR-K-080-100-25-26-B-AAAA	43.20	2	86.40
TOTAL :				2227,97

Table 11

5.6 In-house manufacturing

Some parts of the device must be manufactured in-house. Table 12 and Table 13 list these parts along with the proposed manufacturing methods. The first table focuses on metal components, while the second covers plastic parts produced by additive manufacturing.

Metal parts The part that need to be in metal are listed in Table12 with the type of materials and a proposed manufacturing methods for each part. They are also presented in Figure47b, where they are located on the robot.

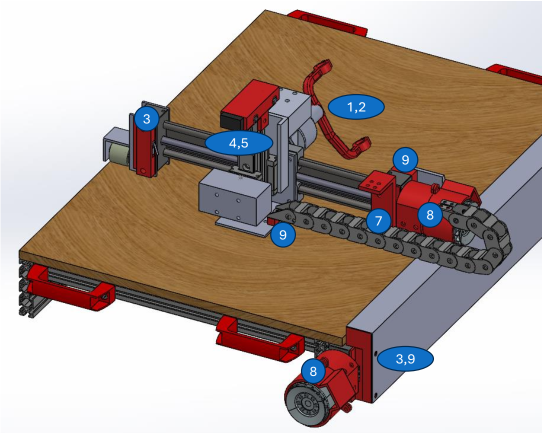

(a) Plastic part location

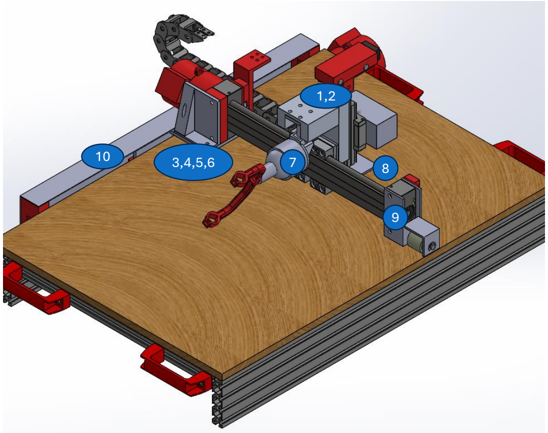

(b) Metal part location

Figure 47: Location of plastic and metal parts in the prototype

Plastic parts All the part to be manufactured in plastic are listed in Table13 and the Figure47a shwo where they are on the robot.

Part name	**Function Position**	**Material**	**Proposed manufacturing method**	**Number**
L-shaped part 1	Interface between the linear guide and sensor	Alu 2024-T3	CNC milling + drilling	1
L-shaped part 2	Interface between linear guide and sensor	Alu 2024-T3	CNC milling + drilling + tapping	2
Link bracket part 1	Connection between actuator Y and X rail	Alu 2024-T3	CNC milling + drilling	3
Link bracket part 2	Connection between X and Y actuator	Alu 2024-T3	CNC milling + drilling	4
Link bracket part 3	Connection between X and Y actuator	Alu 2024-T3	CNC milling + drilling	5
Link bracket part 4	Connection between X and Y actuator	Alu 2024-T3	CNC milling + drilling	6
Ball head support	Mounting point for ball joint under sensor	Alu 2024-T3	CNC milling + drilling	7
Z translation support	Base support for both Z-axis linear guides	Alu 2024-T3	Bending + drilling	8
Wheel support	Connection between the X transmission support and the wheel	Alu 2024-T3	Bending + drilling	9
Y-axis screw cover	Protects the Y transmission from contact and dust	Steel sheet (DC-01)	Laser cutting + bending	10

Table 12: List of in-house machined parts with manufacturing methods and materials

Part name	**Function / Position**	**Material**	**Proposed manufacturing method**	**Number**
Pen holder	Holds the pen tip and connects to the ball head	PLA + carbon fiber	Additive manufacturing (FDM)	1
Pen support ring	Locks the pen inside the holder	PLA	Additive manufacturing (FDM)	2
Endstop sensor support	Holds the endstop sensor on the linear guide	PLA	Additive manufacturing (FDM)	3
Pulley support	Holds the pulley on top of the Z carriage	PLA	Additive manufacturing (FDM)	4
Pulley cover	Covers the pulley and protects the user	PLA	Additive manufacturing (FDM)	5
Contact piece	Activates the endstop sensor	PLA	Additive manufacturing (FDM)	6
Cable carrier support	Provides support for the cable carrier	PLA	Additive manufacturing (FDM)	7
Motor and coupling support	Holds the motor and protects the coupling between motor and lead screw	PLA	Additive manufacturing (FDM)	8
Adjustment shims	Local supports used to fill mechanical gaps or misalignments	PLA	Additive manufacturing (FDM)	9

Table 13: List of 3D printed plastic parts with function and manufacturing method

6 Perspective

This section outlines ideas for future development and areas of interest for improvement. The next major steps in the robot's evolution involve the implementation of the control system and the overall electronic architecture. From a mechanical standpoint, the pen holder design can be further refined as its design does integrate a contact detection, and the motor ventilation may require improvement to ensure proper cooling. A user control panel with start, stop, and emergency buttons could be added, along with a visual interface for feedback or guidance.

The force sensor design may also need revisions and iterations, based on feedback from specialists in the field. The assembly of the full prototype and the definition of a structured test routine represent the immediate priorities. Following the prototype evaluation, targeted upgrades of specific components may be necessary to address any limitations observed during testing. Finally, a critical review of the design choices made throughout the development will help guide future improvements and ensure better performance, safety, and usability.

7 Conclusion

This project focused on physical human-robot interaction (pHRI), a field where robots and humans share tasks in a safe and coordinated way. Safety requirements, both in mechanical design and control strategy, are central to pHRI. To avoid causing harm, robots must be compliant. Indirect admittance control has proven to be a well-suited approach, providing both compliance and adaptability by adjusting the robot's motion based on the forces applied by the user.

Building on these principles, this robot was developed to assist children with dyslexia, particularly those struggling with handwriting. These children often have difficulty forming letters fluently and consistently, which can interfere with spelling and learning, leading to delays in their academic progress. The robot is intended to support the development of motor patterns that allow the child to stop focusing on *how* to draw letters and instead concentrate on *what* to write. This is achieved through a co-manipulation strategy, where the robot shares control of the pen with the child.

Two main interaction modes were defined: transparency and guidance. In transparency mode, the child leads the movement freely and the robot check passively the correctness of the writing. In guidance mode, the robot provides an adjustable level of assistance to guide the child's hand. Key specifications were defined to support these modes: a maximum force of 110 N, a speed of 120 mm/s, and an acceleration of $2\,\mathrm{m/s^2}$. These values were based on real writing data collected from children without dyslexia.

Using the methods proposed in the LMECA2801 Machine Design course, the selected design is a planar Cartesian structure with an additional passive degree of freedom in the Z-axis. It uses a lead screw transmission and includes a raised tabletop to ensure a comfortable arm posture for the child, as the structure does not constrain arm movement or positioning. The pen is custom-designed with two contact points for better force distribution, and a lockable ball joint that allows for orientation adjustment.

A virtual prototype was created using components from suppliers such as Misumi, Igus, and Maxon. Some elements still need to be manufactured at CREDEM to complete the physical prototype and begin real-world testing.

Finally, this project ends on a lighter note. Since the robot is designed to help children learn to write, it seemed fitting to give it a name that reflects this mission. As a small tribute to a great writer—winner of both the Nobel and the Pulitzer prizes—the robot is named **Helpingway**, blending the idea of "helping" and "Hemingway."

Acknowledgements

This work would not have been possible without the support and guidance of several individuals.

First, I would like to express my sincere gratitude to my supervisor, Prof. Ronsse, for his continuous guidance and support throughout the year. I would also like to thank Julien Guiaux Brinon for his valuable assistance during the design phase. My thanks go as well to Benoît Herman for reviewing the design and providing insightful advice to improve the robot.

I am also grateful to Prof. Van Reybroeck for helping me understand the needs and context in which this thesis topic was developed. Finally, I would like to thank Alex Bertholet for his contribution to the design of a sensor used in the project.

Use of AI

AI tools, including ChatGPT, were used for sentence formulation and text fluidity. However, all ideas and content were originally written and reviewed by the student.

1 Writing analysis

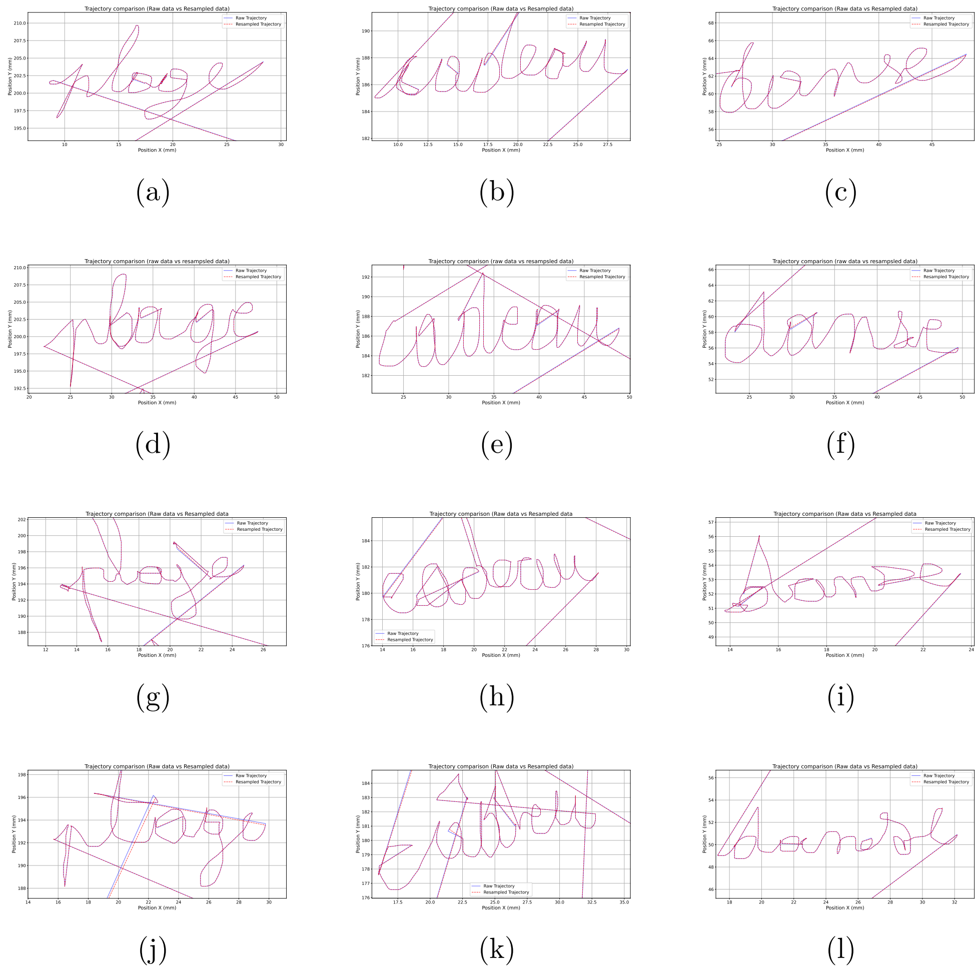

Figure 48: Average size of three words *plage*, *cadeau*, and *papier*, written by four different children. Each row corresponds to a different child, and each column to a different word.

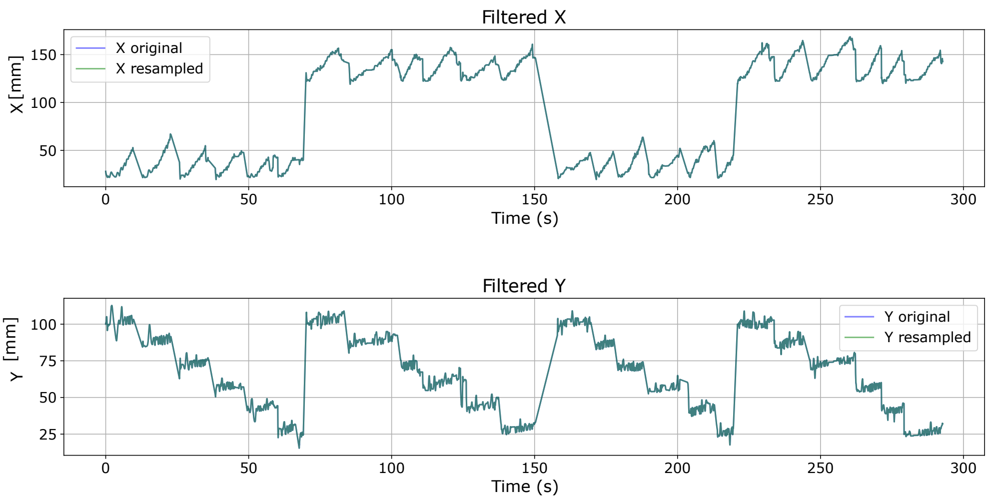

(a)

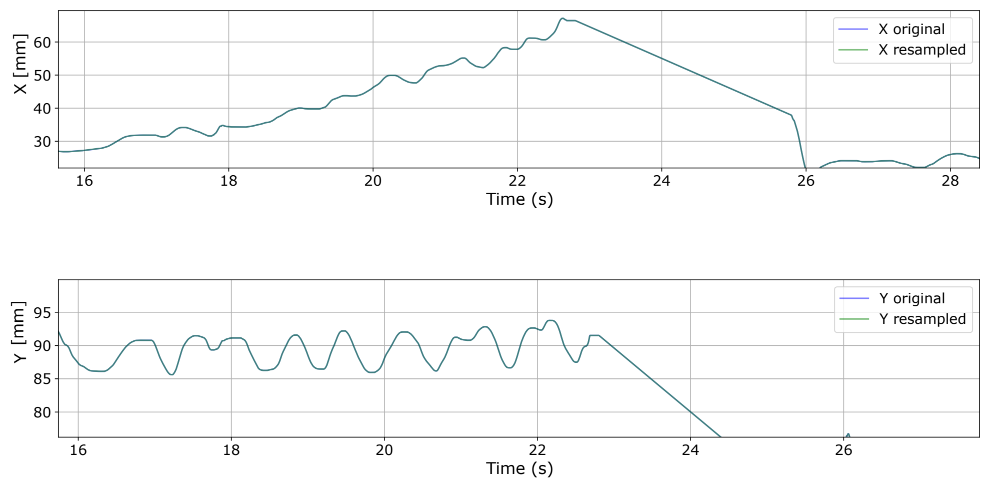

(b)

Figure 49: Position comparison between raw and resampled data and a zoom

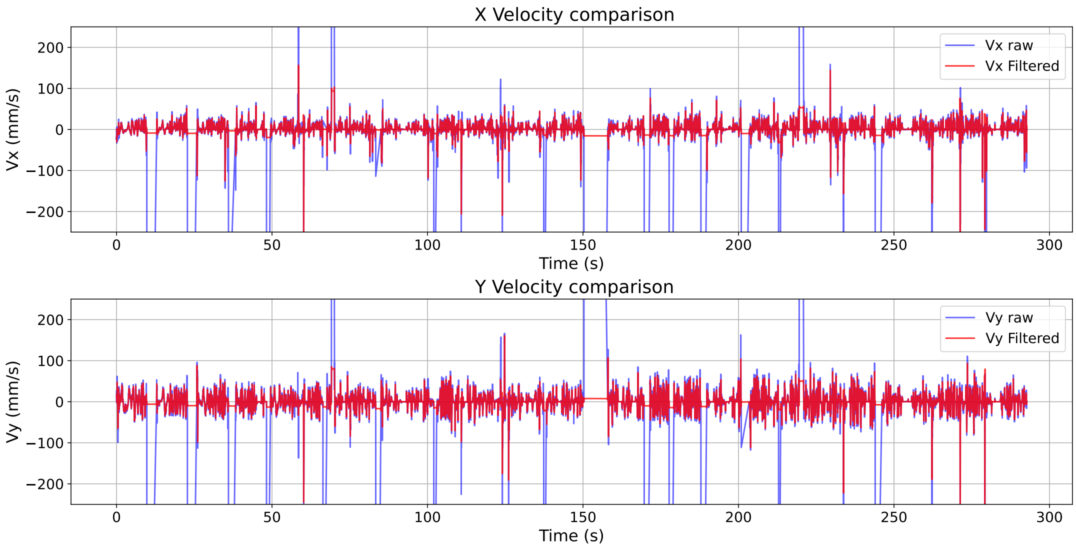

(a)

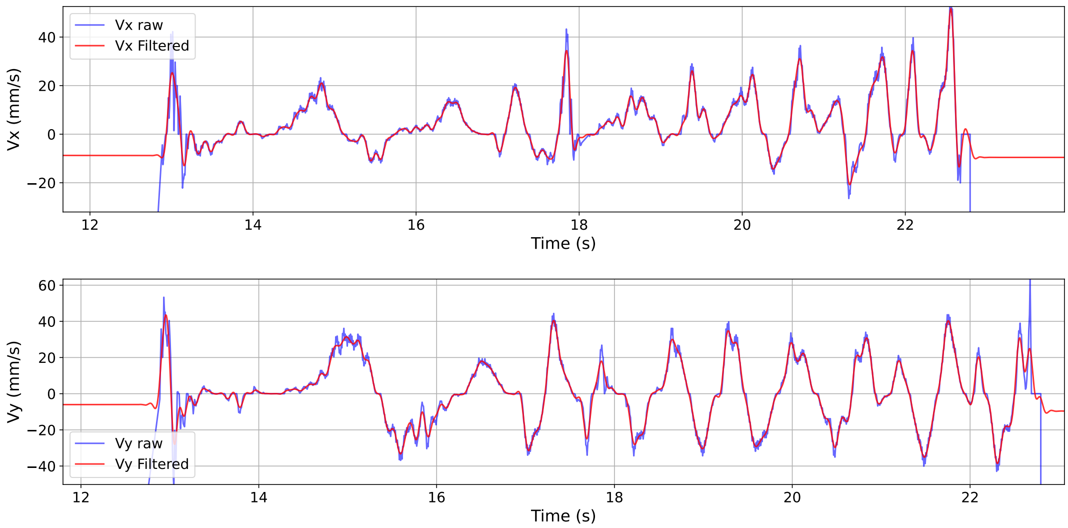

(b)

Figure 50: Velocity comparison between raw and resampled data and a zoom

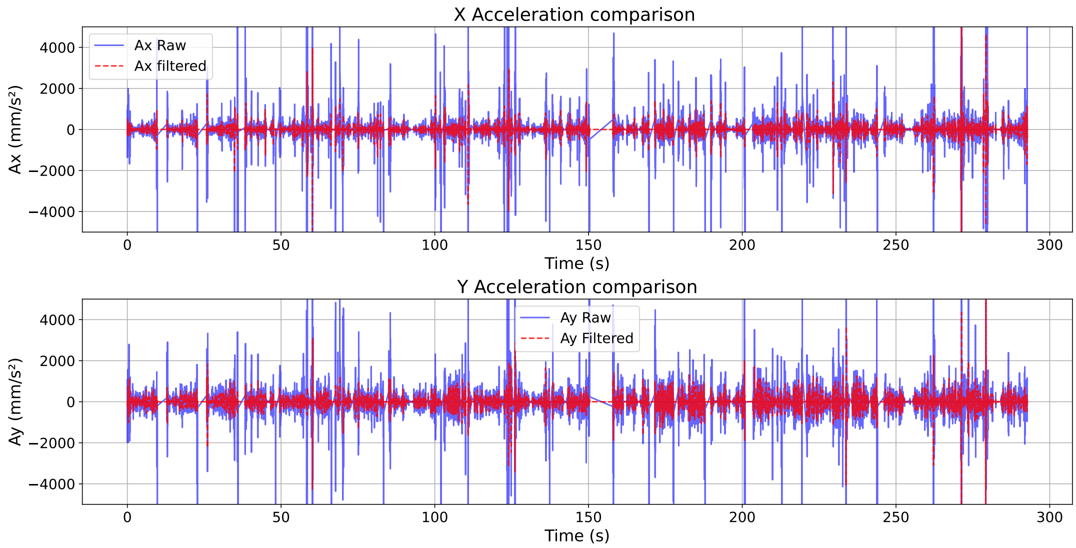

(a)

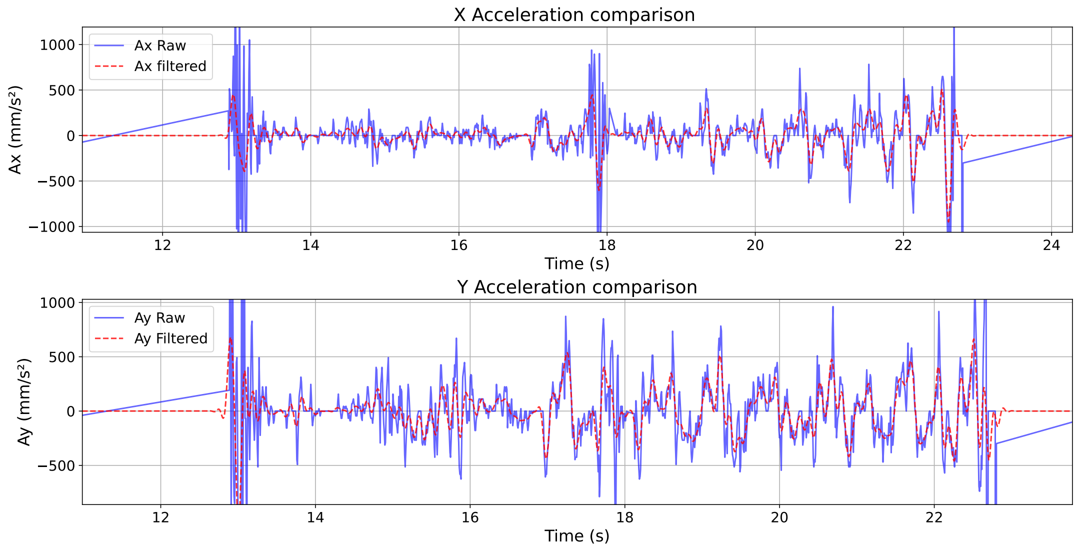

(b)

Figure 51: Acceleration comparison between raw and resampled data and a zoom

2 Motor datasheet

EC 60 flat ∅60 mm, brushless, 200 watt

Ventilated

EC flat

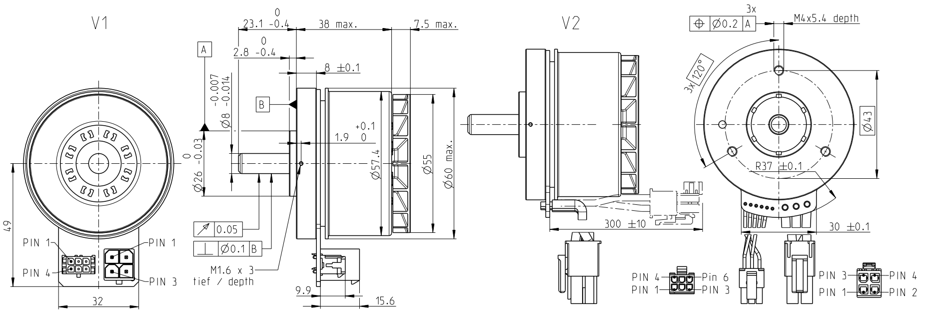

M 1:2

Stock program
Standard program
Special program (on request)

Part numbers			
V1 with Hall sensors	625860	614949	625861
V2 with Hall sensors and cables	647696	642221	647697
Motor data			
Values at nominal voltage			
1 Nominal voltage V	12	24	48
2 No load speed rpm	3760	4300	4020
3 No load current mA	815	497	224
4 Nominal speed rpm	2790	3240	3020
5 Nominal torque mNm	496	540	581
6 Nominal current (max. continuous current) A	15.2*	9.34	4.63
7 Stall torque mNm	2210	2510	2650
8 Stall current A	113	83.2	43.9
9 Max. efficiency %	83.7	85.1	86.1
Characteristics			
10 Terminal resistance phase to phase Ω	0.106	0.288	1.09
11 Terminal inductance phase to phase mH	0.0911	0.279	1.28
12 Torque constant mNm/A	30	52.5	113
13 Speed constant rpm/V	318	182	84.8
14 Speed/torque gradient rpm/mNm	1.13	0.998	0.823
15 Mechanical time constant ms	9.8	8.69	7.17
16 Rotor inertia gcm²	832	832	832

Specifications

Thermal data

17	Thermal resistance housing-ambient	1.22 K/W
18	Thermal resistance winding-housing	0.843 K/W
19	Thermal time constant winding	9.19 s
20	Thermal time constant motor	44 s
21	Ambient temperature	-40...+100°C
22	Max. winding temperature	+125°C

Mechanical data (preloaded ball bearings)

23	Max. speed	6000 rpm
24	Axial play at axial load < 12.0 N	0 mm
	> 12.0 N	0.14 mm
25	Radial play	preloaded
26	Max. axial load (dynamic)	12 N
27	Max. force for press fits (static)	170 N
	(static, shaft supported)	8000 N
28	Max. radial load, 5 mm from flange	112 N

Other specifications

29	Number of pole pairs	7
30	Number of phases	3
31	Weight of motor	360 g

Values listed in the table are nominal.

Connection V1		**V2** (sensors, AWG 24)
Pin 1	Hall sensor 1	Hall sensor 1
Pin 2	Hall sensor 2	Hall sensor 2
Pin 3	Hall sensor 3	Hall sensor 3
Pin 4	GND	GND
Pin 5	V_{Hall} 4.5...24 VDC	V_{Hall} 4.5...24 VDC
Pin 6	N.C.	N.C.
		V2 (Motor, AWG 14)
Pin 1	Motor winding 1	Motor winding 1
Pin 2	Motor winding 2	Motor winding 2
Pin 3	Motor winding 3	Motor winding 3
Pin 4		N.C.

Wiring diagram for Hall sensors see p. 69

Connector	**Part number**	
Molex Micro-Fit	43045-0627	43025-0600
Molex	76829-0104	171692-0104

Connection cable for V1

for windings, L = 3 m **520851**
for Hall sensors, L = 3 m **275878**

Operating range

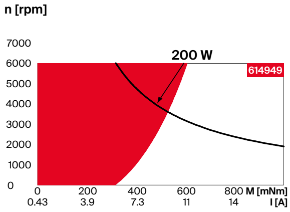

Comments

Continuous operation
In observation of above listed thermal resistance (lines 17 and 18) and an ambient temperature of 25°C, the maximum permissible winding temperature will be reached during continuous operation = thermal limit.

Short term operation
The motor may be briefly overloaded (recurring).

Assigned power rating

Modular system

Details on catalog page 56

Gear
444_GP 52 C
458_GB 80[1]
456_GSW 62 A

Sensor
530_Encoder MILE

Motor Control
547_DEC Module 50/5
551_ESCON Module 50/5
552_ESCON Module 50/8 HE
553_ESCON 70/10
557_ESCON2 Micro 60/5
558_ESCON2 Module 60/12
558_ESCON2 Module 60/30
559_ESCON2 Compact 60/12
559_ESCON2 Compact 60/30

[1]on request
*625860 and 647696 cannot be combined with the MILE encoder, because the current limit of the connectors of the MILE circuit board is 13 A.

Bibliography

[1] S. Haddadin and E. Croft, "Physical human–robot interaction," in *Springer Handbook of Robotics*, B. Siciliano and O. Khatib, Eds., Springer, Cham, 2016, pp. 1835–1874, ISBN: 978-3-319-32550-7. DOI: 10.1007/978-3-319-32552-1_69.

[2] A. De Santis, B. Siciliano, A. De Luca, and A. Bicchi, "An atlas of physical human–robot interaction," *Mechanism and Machine Theory*, vol. 43, no. 3, pp. 253–270, 2008, ISSN: 0094-114X. DOI: https://doi.org/10.1016/j.mechmachtheory.2007.03.003. [Online]. Available: https://www.sciencedirect.com/science/article/pii/S0094114X07000547.

[3] A. De Luca and F. Flacco, "Integrated control for phri: Collision avoidance, detection, reaction and collaboration," in *2012 4th IEEE RAS EMBS International Conference on Biomedical Robotics and Biomechatronics (BioRob)*, 2012, pp. 288–295. DOI: 10.1109/BioRob.2012.6290917.

[4] A. Ajoudani, A. M. Zanchettin, S. Ivaldi, A. Albu-Schäffer, K. Kosuge, and O. Khatib, "Progress and prospects of the human–robot collaboration," *Autonomous Robots*, vol. 42, no. 5, pp. 957–975, 2018. DOI: 10.1007/s10514-017-9677-2.

[5] U. E. Ogenyi, J. Liu, C. Yang, Z. Ju, and H. Liu, "Physical human–robot collaboration: Robotic systems, learning methods, collaborative strategies, sensors, and actuators," *IEEE Transactions on Cybernetics*, vol. 51, no. 4, pp. 1888–1901, 2021. DOI: 10.1109/TCYB.2019.2947532.

[6] W. K. Chung, L.-C. Fu, and S.-H. Hsu, "Motion control," in *Springer Handbook of Robotics*, B. Siciliano and O. Khatib, Eds., Berlin, Heidelberg: Springer, 2008, pp. 133–172, ISBN: 978-3-540-23957-4. DOI: 10.1007/978-3-540-30301-5_7. [Online]. Available: https://doi.org/10.1007/978-3-540-30301-5_7.

[7] C. Ott, R. Mukherjee, and Y. Nakamura, "Unified impedance and admittance control," in *2010 IEEE International Conference on Robotics and Automation*, 2010, pp. 554–561. DOI: 10.1109/ROBOT.2010.5509861.

[8] L. Villani and J. De Schutter, "Force control," in *Springer Handbook of Robotics*, B. Siciliano and O. Khatib, Eds., Springer, Cham, 2016, pp. 195–

220, ISBN: 978-3-319-32550-7. DOI: 10.1007/978-3-319-32552-1_9. [Online]. Available: https://doi.org/10.1007/978-3-319-32552-1_9.
[9] D. Ye, C. Yang, Y. Jiang, and H. Zhang, "Hybrid impedance and admittance control for optimal robot–environment interaction," *Robotica*, vol. 42, no. 2, pp. 510–535, 2024. DOI: 10.1017/S0263574723001601.
[10] I. Rhee, G. Kang, S. J. Moon, *et al.*, "Hybrid impedance and admittance control of robot manipulator with unknown environment," *Intelligent Service Robotics*, vol. 16, no. 1, pp. 49–60, 2023, Received: 03 June 2022; Accepted: 01 December 2022; Published online: 28 December 2022. DOI: 10.1007/s11370-022-00451-5.
[11] C. T. Landi, F. Ferraguti, L. Sabattini, C. Secchi, and C. Fantuzzi, "Admittance control parameter adaptation for physical human-robot interaction," in *2017 IEEE International Conference on Robotics and Automation (ICRA)*, 2017, pp. 2911–2916. DOI: 10.1109/ICRA.2017.7989338.
[12] A. Q. L. Keemink, H. van der Kooij, and A. H. A. Stienen, "Admittance control for physical human–robot interaction," *The International Journal of Robotics Research*, pp. 1–24, 2018. DOI: 10.1177/0278364918768950.
[13] K. Wen, D. Necsulescu, and J. Sasiadek, "Haptic force control based on impedance/admittance control," *IFAC Proceedings Volumes*, vol. 38, no. 1, pp. 427–432, 2005, 16th IFAC World Congress, ISSN: 1474-6670. DOI: https://doi.org/10.3182/20050703-6-CZ-1902.01341. [Online]. Available: https://www.sciencedirect.com/science/article/pii/S1474667016373530.
[14] E. M. S. Laboratories. "Axidraw writing and drawing machines." Accessed: April 2025. [Online]. Available: https://axidraw.com/.
[15] iDraw Pen Plotter. "Idraw h pen plotter." Accessed: April 2025. [Online]. Available: https://idrawpenplotter.com/shop/ols/products/idraw-pen-plotter-h-version-a3.
[16] G. Cover. "Maxwriter double parallel scara drawing robot." Accessed: April 2025. [Online]. Available: https://www.general-cover.com/Mai-Maxwriter.html.
[17] I. Breton and A. Campeau-Lecours, "Development of a robotic handwriting assistant for children with movement disorder," *Acta Tecnología*, vol. 10, no. 2, pp. 73–79, 2024, Received: 12 June 2024; Revised: 21 June 2024; Accepted: 27 June 2024, ISSN: 2453-675X. DOI: 10.22306/atec.v10i2.203.
[18] M. C. Robots. "Makelangelo art robot." Accessed: April 2025. [Online]. Available: https://www.marginallyclever.com/shop/robots/drawing-robots/makelangelo-5/.
[19] 3. Systems. "Geomagic touch haptic device." Accessed: April 2025. [Online]. Available: https://www.3dsystems.com/haptics-devices/touch.

[20] Haption. “Virtuose 3d desktop - haptic device.” Accessed: April 2025. [Online]. Available: https://cornershop-immersion.com/en/capture-interaction/161-virtuose-3d-desktop.html.

[21] Axinesis, *REAplan – Robot de rééducation du membre supérieur*, https://www.axinesis.com/fr/nos-solutions/reaplan/, Accessed May 2025, 2025.

[22] MIT News Office, *Robot proves effective in physical therapy for stroke victims*, https://news.mit.edu/2000/manus-0607, Accessed May 2025, 2000.

[23] Tecnalia, *ArmAssist – Robot assistant pour la rééducation des membres supérieurs*, https://www.tecnalia.com/fr/actifs-technologiques/armassist-robot-assistant-pour-la-reeducation-des-membres-superieurs, Accessed May 2025, 2025.

[24] Syrebo Care, *SYREBO Upper Limb Rehabilitation Robot SY-UEA2*, https://syrebocare.com/en-be/products/syrebo-upper-limb-rehabilitation-robot-sy-uea2, Accessed May 2025, 2025.

[25] Medimex, *Armeo Power – Rééducation du membre supérieur*, https://www.medimex.fr/produit/armeo-power-reeducation-membre-superieur/, Accessed May 2025, 2025.

[26] G. R. Lyon, S. E. Shaywitz, and B. A. Shaywitz, “Defining dyslexia, comorbidity, teachers’ knowledge of language and reading: A definition of dyslexia,” *Annals of Dyslexia*, vol. 53, pp. 1–14, 2003. DOI: 10.1007/s11881-003-0001-9. [Online]. Available: http://dx.doi.org/10.1007/s11881-003-0001-9.

[27] A. Notarnicola, P. Angelelli, A. Judica, and P. Zoccolotti, “Development of spelling skills in a shallow orthography: The case of italian language,” *Reading and Writing - READ WRIT*, vol. 25, May 2012. DOI: 10.1007/s11145-011-9312-0.

[28] C. Di Brina, R. Averna, P. Rampoldi, S. Rossetti, and R. Penge, “Reading and writing skills in children with specific learning disabilities with and without developmental coordination disorder,” *Motor Control*, vol. 22, pp. 1–15, Feb. 2018. DOI: 10.1123/mc.2016-0006.

[29] E. Blampain, C. Gosse, and M. V. Reybroeck, “Copying skills in children with and without dyslexia,” *Reading and Writing*, vol. 34, pp. 859–885, 2021. DOI: 10.1007/s11145-020-10094-6. [Online]. Available: https://doi.org/10.1007/s11145-020-10094-6.

[30] C. Gosse and M. V. Reybroeck, “Do children with dyslexia present a handwriting deficit? impact of word orthographic and graphic complexity on handwriting and spelling performance,” *Research in Developmental Disabilities*, vol. 97, p. 103 553, 2020, Epub 2019 Dec 13. DOI: 10.1016/j.ridd.2019.103553. [Online]. Available: https://doi.org/10.1016/j.ridd.2019.103553.

[31] C. Gosse, S. Carbonnelle, C. de Vleeschouwer, *et al.*, "Specifying the graphic characteristics of words that influence children's handwriting," *Reading and Writing*, vol. 31, pp. 1181–1207, May 2018. DOI: 10.1007/s11145-018-9834-9.
[32] C. Gosse, L. Dricot, and M. Van Reybroeck, "Evidence of graphomotor dysfunction in children with dyslexia: A combined behavioural and fmri experiment," *Cortex*, vol. 148, pp. 68–88, 2022, ISSN: 0010-9452. DOI: https://doi.org/10.1016/j.cortex.2021.11.021. [Online]. Available: https://www.sciencedirect.com/science/article/pii/S001094522200003X.
[33] M. V. Reybroeck and N. Michiels, "Finger-writing intervention impacts the spelling and handwriting skills of children with developmental language disorder: A multiple single-case study," *Reading and Writing*, vol. 31, pp. 1319–1341, 2018. DOI: 10.1007/s11145-018-9845-6. [Online]. Available: https://doi.org/10.1007/s11145-018-9845-6.
[34] M. J. McKay *et al.*, "Normative reference values for strength and flexibility of 1,000 children and adults," *Neurology*, vol. 88, no. 1, pp. 36–43, Jan. 2017, Epub 2016 Nov 23. DOI: 10.1212/WNL.0000000000003466.
[35] Oriental Motor, *Ball and lead screw sizing tool*, Accessed: 2025-05-16, 2024. [Online]. Available: https://www.orientalmotor.com/motor-sizing/ballLeadScrew-sizing.html#QuickReport.
[36] Igus GmbH, *Material data for linear guides*, Accessed: 2025-05-16, 2024. [Online]. Available: https://www.igus.fr/info/linear-guides-material-data.
[37] Igus GmbH, *Efficiency: What does this mean for lead screws?* Accessed: 2025-05-16, 2022. [Online]. Available: https://blog.igus.eu/efficiency/.
[38] Maxon Support, *Meaning and impact of cogging torque and ripple torque*, Accessed: 2025-05-16, 2022. [Online]. Available: https://support.maxongroup.com/hc/en-us/articles/6726327972252-Meaning-and-impact-of-Cogging-torque-and-Ripple-torque.

UNIVERSITÉ CATHOLIQUE DE LOUVAIN
École polytechnique de Louvain
Rue Archimède, 1 bte L6.11.01, 1348 Louvain-la-Neuve, Belgique | **www.uclouvain.be/epl**